



Observed trends in ground-level O₃ in Monterrey, Mexico, during 1993–2014: comparison with Mexico City and Guadalajara

Iván Y. Hernández Paniagua^{1,2}, Kevin C. Clemitshaw³, and Alberto Mendoza¹

¹Escuela de Ingeniería y Ciencias, Tecnológico de Monterrey, Campus Monterrey, Av. Eugenio Garza Sada 2501, Monterrey, N.L., 64849, México

²Centro de Ciencias de la Atmosfera, Universidad Nacional Autónoma de México, Ciudad de México, México

³Department of Earth Sciences, Royal Holloway University of London, Egham, Surrey TW20 0EX, UK

Correspondence to: A. Mendoza (mendoza.alberto@itesm.mx)

Received: 20 July 2016 – Discussion started: 12 September 2016

Revised: 25 May 2017 – Accepted: 15 June 2017 – Published: 31 July 2017

Abstract. Here, we present an assessment of long-term trends in O₃ and odd oxygen (O₃ + NO₂) at the industrial Monterrey metropolitan area (MMA) in NE Mexico. Diurnal amplitudes in O_x (AV_d) are used as a proxy for net O₃ production, which is influenced by the NO₂ photolysis rate. No significant differences in the AV_d are observed between weekends and weekdays, although the largest AV_d values are observed at sites downwind of industrial areas. The highest O₃ mixing ratios are observed in spring, with minimum values in winter. The largest annual variations in O₃ are typically observed downwind of the MMA, with the lowest variations generally recorded in highly populated areas and close to industrial areas. A wind sector analysis of mixing ratios of O₃ precursors revealed that the dominant sources of emissions are located in the industrial regions within the MMA and surrounding area. Significant increasing trends in O₃ in spring, summer, and autumn are observed depending on site location, with trends in annual averages ranging between 0.19 and 0.33 ppb yr⁻¹. Overall, from 1993 to 2014, within the MMA, O₃ has increased at an average rate of 0.22 ppb yr⁻¹ ($p < 0.01$), which is in marked contrast with the decline of 1.15 ppb yr⁻¹ ($p < 0.001$) observed in the Mexico City metropolitan area (MCMA) for the same period. No clear trend is observed from 1996 to 2014 within the Guadalajara metropolitan area (GMA).

1 Introduction

O₃ is a secondary air pollutant formed in the troposphere via the photo-oxidation of CO, methane (CH₄), and volatile organic compounds (VOCs) in the presence of NO and NO₂ (NO + NO₂ = NO_x) (Jenkin and Clemitshaw, 2000). The system of O₃ production is not linear and is termed NO_x-limited, when O₃ production increases in response to increasing NO_x emissions and termed VOC-limited when it responds positively to emissions of VOCs (Monks et al., 2015; Pusede et al., 2015). Tropospheric O₃ is of concern to policy makers due to its adverse impacts on human health, agricultural crops, and vegetation and also due to its role as a greenhouse gas despite its relatively short lifetime of around 22.3 ± 3.0 days (Stevenson et al., 2006; IPCC, 2013; WHO, 2014; Lelieveld et al., 2015). As the predominant source of OH, tropospheric O₃ controls the lifetime of CH₄, CO, and VOCs, among many other air pollutants (Revell et al., 2015). In polluted regions, increased levels of O₃ are prevalent during seasons with stable high-pressure systems and intense photochemical processing of NO_x and VOCs (Dentener et al., 2005; Xu et al., 2008) with downward transport from the stratosphere of lesser importance (Wang et al., 2012). By contrast, the main removal processes for tropospheric O₃ are chemical loss and dry deposition (Atkinson, 2000; Jenkin and Clemitshaw, 2000).

Tropospheric O₃ increased in the Northern Hemisphere (NH) during 1950–1980 due to rapid increases in precursor emissions during the industrialisation and economic growth of Europe and North America (NA) (Staehelin and Schmid,

1991; Guicherit and Roemer, 2000). Since the 1990s, reductions in O₃ precursor emissions in economically developed countries have resulted in decreases in tropospheric O₃ levels (Schultz and Rast, 2007; Butler et al., 2012; Pusede et al., 2012); however, in some regions, increases in O₃ have also been reported. For instance, from an analysis of O₃ data from 179 urban sites over France during 1999–2012, Sicard et al. (2016) reported an increasing trend in the annual averages of 0.14 ± 0.19 ppb yr⁻¹, and in the medians of 0.13 ± 0.22 ppb yr⁻¹, attributed to long-range transport and reduced O₃ titration by NO due to reductions in local NO_x emissions. However, Sicard et al. (2016) also reported during the same period that at 61 rural sites, O₃ decreased in the annual averages by 0.12 ± 0.21 ppb yr⁻¹ and in the medians by 0.09 ± 0.22 ppb yr⁻¹.

In the US and Canada, O₃ levels have decreased substantially at different metrics during the last 2 decades in response to more stringent emissions controls focused on on-road and industrial sources. In the greater area of Toronto from 2000 to 2012, O₃ levels decreased at urban sites by approximately 0.4 % yr⁻¹, and at suburban sites by approximately 1.1 % yr⁻¹, as a consequence of a reduction in the midday averages of NO₂ of 5.8–6.4 % yr⁻¹ and in the VOC reactivity of 9.3 % yr⁻¹ (Pugliese et al., 2014). Emissions estimates suggest an overall national scale decrease during 1980–2008 in US NO_x and VOCs emissions of 40 and 47 %, respectively, with city-to-city variability (EPA, 2009; Xing et al., 2013). Lefohn et al. (2010) reported that for 12 US major metropolitan areas, the O₃ US EPA exposure metrics of the annual second highest 1 h average and the annual fourth highest daily maximum 8 h average decreased during 1980–2008 at 87 and 71 % of the monitoring sites evaluated, respectively. However, Lefohn et al. (2010) observed an increase in the lower- and mid-O₃ mixing ratios in response to decreased titration by NO. More recently, Simon et al. (2015) assessed changes in the 1 h average O₃ mixing ratios at around 1400 sites across the US between 1998 and 2013, using the 5th, 25th, 50th, 75th, and 95th percentiles and the maximum daily 8 h average. Overall, Simon et al. (2015) observed increases at the lower end of the O₃ data distribution of 0.1–1 ppb yr⁻¹, mostly in urban and suburban areas, whereas O₃ decreased at the upper end of the data distribution between 1 and 2 ppb yr⁻¹ in less urbanised areas. Such changes were associated with the implementation of control strategies within the US, such as the NO_x SIP call, and tighter point and vehicle emissions standards to abate peak O₃ mixing ratios.

In Mexico, studies of long-term trends in O₃ have focused on the Mexico City metropolitan area (MCMA) (Molina and Molina, 2004; Jaimes et al., 2012; Rodríguez et al., 2016), with reports of a decrease in O₃ annual averages of ca. 33 % during the last 2 decades (Parrish et al., 2011; SEDEMA, 2016a). O₃ has received less consideration in other large metropolitan areas, where Mexican air quality standards are frequently exceeded (Table 1). Indeed, since 2000, recorded

O₃ mixing ratios have exceeded Mexican official standards for 1 h average (110 ppb) and 8 h running average (80 ppb) O₃ by more than 50 % in the Guadalajara metropolitan area (GMA, the second most populated city) and in the Monterrey metropolitan area (MMA, the third most populated city) (INE, 2011; SEMARNAT, 2015). To date, only Benítez-García et al. (2014) have addressed changes in ambient O₃ in the GMA and MMA during 2000–2011, reporting an increase in O₃ annual averages of around 47 and 42 %, respectively. However, it should be noted that the ordinary linear regression analysis used by Benítez-García et al. (2014) may be biased by extreme values and is therefore not suitable to determine long-term O₃ trends with significant confidence.

To improve air quality, the Mexican government has introduced several initiatives to reduce primary pollutant emissions, with emissions estimates reported in the Mexican National Emissions Inventory (NEI). The NEI suggests that from 1999 to 2008, anthropogenic NO_x emissions decreased in the MCMA by 3.8 % yr⁻¹, but increased in the GMA and the MMA by 1.9 and 4.0 % yr⁻¹, respectively (Fig. S1 in the Supplement) (SEMARNAT, 2006, 2011, 2014). These NEI NO_x emissions estimates agree with the decrease for the MCMA of 1.7 % yr⁻¹ in the NO₂ vertical column density during 2005–2014 reported by Duncan et al. (2016), but disagree for the GMA and the MMA where decreases of 2.7 % yr⁻¹ and of 0.3 % yr⁻¹, respectively, are reported. Similarly, Boersma et al. (2008) observed that NO_x emissions over Mexico derived from NO₂ satellite observations were higher by a factor of 1.5–2.5 times than bottom-up emissions estimates, which were lower by a factor of 1.6–1.8 than data reported in the NEI 1999 base year. The NEI anthropogenic VOC emissions estimates suggest a decrease in the MMA by 0.2 % yr⁻¹ but increases in the MCMA and in the GMA by 2.7 % yr⁻¹ and by 3.2 % yr⁻¹, respectively (Fig. S1) (SEMARNAT, 2006, 2011, 2014). However, as for NO_x, NEI trends in VOCs disagree with existing reports for average VOC decreases within the MCMA (Arriaga-colina et al., 2004; Garzón et al., 2015).

Local authorities have developed local emissions inventories for the MCMA and the MMA, although only for the MCMA have the inventories been compiled with a frequency of 2 years since 1996 (SEDEMA, 1999, 2001, 2003, 2004, 2006, 2008, 2010, 2012, 2014, 2016b; SDS, 2015). The accuracy of the MCMA emissions inventories has also been assessed during several field campaigns. For instance, during the MCMA 2002–2003 campaign, Velasco et al. (2007) observed an overestimation in the 1998 inventory for VOC emissions of alkenes and aromatics but an underestimation in the contribution of some alkanes. By contrast, for the 2002 MCMA inventory, Lei et al. (2007) reported an underestimation in the VOC total emissions of around 65 %, based on a simulation of an O₃ episode that occurred in 2003 within the MCMA. Therefore, since these emissions estimates are used to predict future air quality and to design clean air poli-

Table 1. Air quality limit values stated in Mexican legislation.

Pollutant	Mexican official standard	Limit value ^a
O ₃ (ppb)	NOM-020-SSA1-1993	110 (1 h), 80 (8 h) ^{b, c}
	NOM-020-SSA1-2014	95 (1 h), 70 (8 h) ^{b, c}
PM ₁₀ (µg m ⁻³)	NOM-025-SSA1-1993	75 (24 h), 40 (1 yr)
	NOM-025-SSA1-2014	50 (24 h), 35 (1 yr)
PM _{2.5} (µg m ⁻³)	NOM-025-SSA1-1993	45 (24 h), 12 (1 yr)
	NOM-025-SSA1-2014	30 (24 h), 10 (1 yr)
CO (ppm)	NOM-02-SSA1-1993	11 (8 h) ^c
NO ₂ (ppm)	NOM-023-SSA1 – 1993	0.21 (1 h)

^a Average period. ^b Not to be exceeded more than four times in a calendar year. ^c Running average.

cies, it is imperative to examine the results of the policies implemented to control emissions of O₃ precursors.

To our knowledge, no previous study has addressed trends in O₃ and odd oxygen in urban areas of Mexico. In this study, we describe trends in ground-level O₃ within the MMA and its response to changes in precursor emissions during 1993–2014. Long-term and high-frequency measurements of O₃ were recorded at five air quality monitoring stations evenly distributed within the MMA. In order to better assess photochemical production of O₃, odd oxygen defined as ([O_x] = [O₃] + [NO₂]) was also considered, as O₃ and NO₂ are rapidly interconverted. Diurnal and annual cycles of O₃ and O_x are used to interpret net O₃ production within the MMA. We show that air mass origin strongly influences the O₃ annual increases. The trends in O₃, O_x, and precursor emissions are compared with those observed within the MCMA and GMA. Finally, we describe how NEI emissions estimates for NO_x and VOCs disagree in the trend magnitudes with ground-based NO_x and VOCs measurements made in the urban areas studied here.

This paper is organised as follows: Sect. 2 presents the data quality and methodology used to derive the different trends presented. Section 3 describes in detail the O₃ and O_x diurnal and annual cycles and annually and seasonally averaged trends. Section 4 discusses the origin of the O₃ and O_x diurnal variations and trends in the light of changes in precursor emissions. Finally, Sect. 5 provides some conclusions regarding the trends observed in the urban areas studied.

2 Methodology

2.1 Monitoring of O₃ in the Monterrey metropolitan area (MMA)

The MMA (25°40′ N, 100°20′ W) is located around 720 km N of Mexico City, some 230 km S of the US border in the state of Nuevo León (Fig. 1a). It lies at an average altitude of

500 m a.s.l. and is surrounded by mountains to the S and W, with flat terrain to the NE (Fig. 1b). The MMA is the largest urban area in northern Mexico at around 4030 km² and is the third most populous area in the country with 4.16 million inhabitants, which in 2010, comprised 88 % of the population of Nuevo León State (INEGI, 2010). It is the second most important industrial area in Mexico and has the highest gross domestic product per capita (Fig. 1c). Although the weather changes rapidly on a daily timescale, the climate is semi-arid with an annual average rainfall of 590 mm and an annual average temperature of 25.0 °C with hot summers and mild winters (ProAire-AMM, 2008; SMN, 2016).

Within the MMA, tropospheric O₃, six additional air pollutants (CO, NO, NO₂, SO₂, PM₁₀, and PM_{2.5}), and seven meteorological parameters (wind speed (WS), wind direction (WD), temperature (Temp), rainfall, solar radiation (SR), relative humidity (RH), and pressure) have been monitored continuously, with data summarised as hourly averages, since November 1992 at five stations that form part of the Integral Environmental Monitoring System (SIMA) of the Nuevo León State Government (Table 2; SDS, 2016). From November 1992 to April 2003, and in accordance with EPA EQOA-0880–047, Thermo Environmental Instruments Inc. (TEI) model 49 UV photometric analysers were used to measure O₃ with a stated precision of less than ±2 ppb O₃ and a detection limit of 2 ppb O₃. Similarly, in accordance with RFNA-1289–074, TEI model 42 chemiluminescence detectors were used to measure NO-NO₂-NO_x with a stated precision of less than ±0.5 ppb NO and a detection limit of 0.5 ppb NO. In May 2003, replacement TEI model 49C O₃ and model 42C NO-NO₂-NO_x analysers were operated as above, with a stated precision of better than ±1 ppb O₃ and ±0.4 ppb NO and detection limits of 1 ppb O₃ and 0.4 ppb NO. To rule out instrumentation influences on the air pollutant trends determined, long-term trends based on annual averages were compared with those derived using 3-year running averages, in accordance with Parrish et al. (2011) and Akimoto

Table 2. Site description and location of the five monitoring sites within the MMA.

Site	Code	Location	Elevation (m a.s.l.)	Site description
Guadalupe	GPE	25°40.110' N, 100°14.907' W	492	Urban background site in the La Pastora park, surrounded by a highly populated area, 450 m from Pablo Rivas Rd.
San Nicolás	SNN	25°44.727' N, 100°15.301' W	476	Urban site surrounded by a large number of industries and residential areas, 450 m from Juan Diego Díaz de Berlagna Rd.
Obispado	OBI	25°40.561' N, 100°20.314' W	560	Urban site near the city centre of MMA, 250 m from José Eleuterio González Rd. and 250 m from Antonio L. Rodríguez Rd.
San Bernabé	SNB	25°45.415' N, 100°21.949' W	571	Urban site in a residential area downwind of an industrial area with high traffic volume, 140 m from Aztlán Rd.
Santa Catarina	STA	25°40.542' N, 100°27.901' W	679	Urban site downwind of industrial sources, 200 m from Manuel Ordóñez Rd.

et al. (2015) (Supplement Sect. S1.1; Fig. S2). Calibration, maintenance procedures, and quality assurance/quality control (QA/QC) followed protocols established in the Mexican standards NOM-036-SEMARNAT-1993 and NOM-156-SEMARNAT-2012. The SIMA data set has been validated by the Research Division of Air Quality of the Secretariat of Environment and Natural Resources (SEMARNAT). The monitoring of O₃ and other air pollutants in the MCMA and the GMA is detailed in the Supplement Sect. S1.2–3.

2.2 NEI data

NEI data for estimated NO_x and VOC emissions for the 1999, 2005, and 2008 base years were obtained from the SEMARNAT website (<http://sinea.semarnat.gob.mx>). The data comprised emissions sources (mobile, point, area, and natural) and air pollutants (NO_x, VOCs, SO_x, CO, PM_{2.5}, and PM₁₀) on national, state, and municipality scales. The NEI emissions estimates are developed in accordance with the Manual for the Emission Inventories Program of Mexico (Radian, 2000), which is based on the US EPA AP-42 emissions factors categorisation (EPA, 1995). The emissions factors are regionalised for each Mexican state, based upon on-site measurements and survey information. Updates to the emissions factors have been conducted for each released NEI, although no changes in the methodology were implemented between the 1999 and 2008 base years. Overall, the mobile emissions were estimated using the MOBILE6-Mexico model (EPA, 2003). The emissions from point sources were derived using the annual operation reports submitted to SEMARNAT. The emissions from area sources were obtained using the categorisation of Mexican area sources and the regionalised AP-42 emissions factors.

The MCMA emissions inventories have been developed with a 2-year frequency since 1996 and were obtained from the MCMA Environment Secretariat website (<http://www.aire.cdmx.gob.mx/>). The methodology used to construct the MCMA inventory estimates is consistent with that used in the NEI (SEDEMA, 2016a), which is based on the AP-42

EPA emissions factors. However, more speciated emissions factors have been developed in each released version, considering updates in the local industrial activity, survey information, and field measurement campaigns. To date, the only significant change in the methodology is the replacement of the Mobile6-Mexico model with the MOVES model to obtain the 2014 base year mobile emissions (SEDEMA, 2016b). As for the MCMA inventories, more speciated emissions factors than those contained in the NEI were developed to produce the MMA emissions inventory 2013 base year (SDS, 2015); although, estimates of mobile emissions were obtained with the Mobile6-Mexico model (EPA, 2003).

2.3 Analytical methods

SIMA, SIMAT (Atmospheric Monitoring System of the MCMA), and SIMAJ (Atmospheric Monitoring System of the GMA) instrumentation recorded O₃ data every minute, which were then validated and archived as 1 h averages. Total SIMA O₃ data capture by year and site is shown in Fig. S3. Data capture averaged during 1993–2014 ranged from 82.6 % at GPE (see Table 2 for all site abbreviations) to 93.3 % at SNB, with data capture < 50 % during 1998–2000 at GPE, in 1998 at SNN, and in 1999 at OBI. A threshold of 75 % data capture was defined to consider data valid and representative (ProAire-MMA, 2008; Zellweger et al., 2009; Wilson et al., 2012). All data were processed with hourly averages used to determine daily averages, which were used to calculate monthly averages, from which yearly averages were obtained.

2.4 Data analysis methods

The SIMA, SIMAT, and SIMAJ O₃ data sets were analysed extensively using the openair package v1.1–4 (Carslaw and Ropkins, 2012) for R software v3.1.2 (R Core Team, 2013). In this study, the openair functions windRose, timeVariation, and TheilSen were used to analyse air pollution data. Briefly, the windRose summarises wind speed and wind direction by a given timescale, with proportional paddles represent-

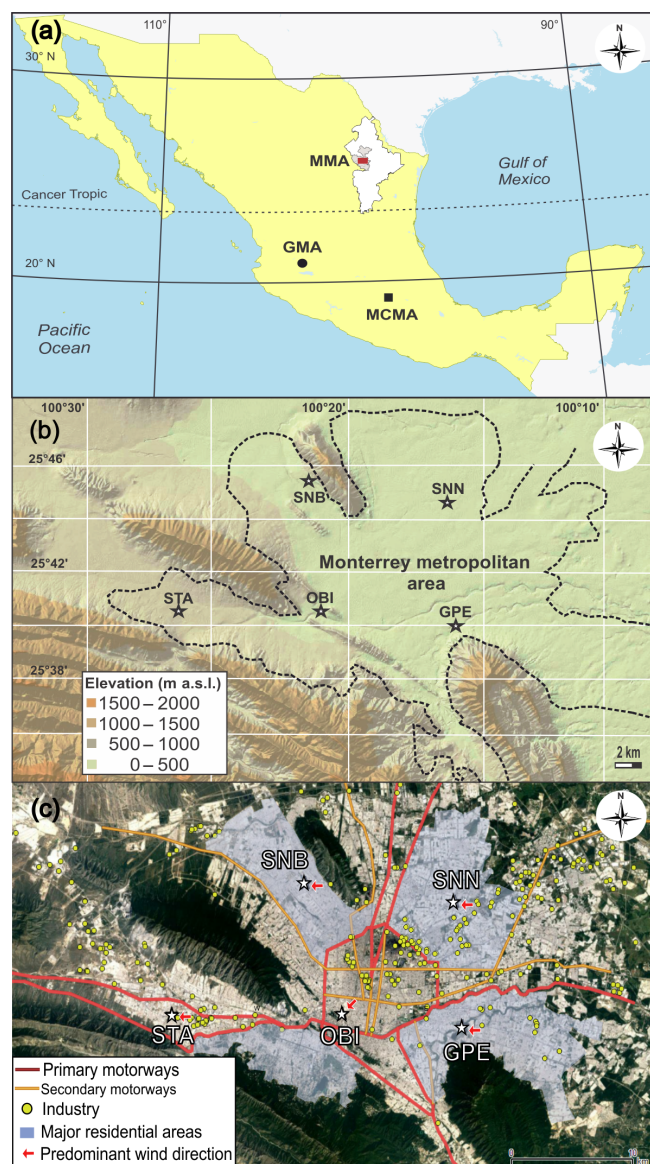


Figure 1. (a) The MMA, MCMA, and GMA in the national context. (b) Topography of the MMA and distribution of the five monitoring sites over the area. (c) The five monitoring sites in relation to primary and secondary motorways, industries, and major residential areas. The red arrows show the predominant wind direction at each site from 1993 to 2014.

ing the percentage of wind occurrence from a certain angle and speed range. The timeVariation function was used to obtain normalised daily cycles by season, and weekly cycles, with the 95 % confidence intervals in the cycles calculated from bootstrap resampling, which accounts for better estimations for non-normally distributed data (Carslaw, 2015). Finally, long-term trends in air pollutants in the MCMA, GMA, and MMA were computed with the TheilSen function, which is based on the non-parametric Theil-Sen method (Carslaw, 2015; and references therein). The Theil-Sen estimate of the

slope is the median of all slopes calculated for a given n number of x , y pairs, while the regression parameters, confidence intervals, and statistical significance are determined through bootstrap resampling. It yields accurate confidence intervals despite the data distribution and heteroscedasticity and is also resistant to outliers.

The trends computed with openair were contrasted with those calculated using the MAKESENS 1.0 macro (Salmi et al., 2002) as follows. Firstly, the presence of a monotonic trend was tested with the non-parametric Mann–Kendall test. For the MCMA, GMA, and MMA, the available yearly data are $n > 10$; hence, positive values in the Z parameter correspond to positive trends and vice-versa for negative values of Z . The significance of the estimated trend was tested at $\alpha = 0.001, 0.01, 0.05,$ and 0.1 using a two-tailed test. Secondly, slopes of linear trends were calculated with the non-parametric Sen’s method, which assumes linear trends, with a Q slope and a B intercept. To calculate Q , first the slopes of all data values were calculated in pairs, with the Sen’s estimator slope as the median of all calculated slopes. Finally, $100(1 - \alpha) \%$ two-sided confidence intervals about the slope estimate were obtained based on a normal distribution. Comparisons of estimated trends from both approaches are shown in the Supplement Sect. S1.4 (Fig. S4).

The O₃ and other air pollutant time series were decomposed into trend, seasonal, and residual components using the seasonal trend decomposition technique (STL; Cleveland et al., 1990). STL consists of two recursive procedures: an inner loop nested inside an outer loop, assuming measurements of x_i (independent) and y_i (dependent) for $i = 1$ to n . The seasonal and trend components are updated once in each pass through the inner loop; each complete run of the inner loop consists of $n_{(i)}$ such passes. Each pass of the outer loop consists of the inner loop followed by a computation of the robustness weights, which are used in the following run of the inner loop to minimise the influence of transient and aberrant behaviour on the trend and seasonal components. The initial pass of the outer loop is performed with all robustness weights equal to 1, followed by $n_{(0)}$ passes of the outer loop. The Kalman smoother (KS) was used to provide minimum-variance unbiased linear estimations of observations and to impute missing data to satisfy the STL (Reinsel, 1997; Durbin and Koopman, 2012; Carslaw, 2015). Overall, statistical seasonal autoregressive and moving averages with annual seasonal components were employed. Statistical analyses were carried out with SPSS 19.0.

In order to carry out seasonal analyses of data, seasons were defined according to temperature records in the NH, as described previously (Hernández-Paniagua et al., 2015): winter (December–February), spring (March–May), summer (June–August), and autumn (September–November). Wind-sector analyses of data were performed by defining eight wind sectors each of 45° starting from $0 \pm 22.5^\circ$. The lower bound of each sector was established by adding 0.5° to avoid data duplicity. Data were assigned to a calm sector

when wind speed was $\leq 0.36 \text{ km h}^{-1}$ (0.1 m s^{-1}). To assess regional transport, air mass back trajectories (AMBTs) were calculated using the HYSPLIT model v.4 (NOAA Air Resources Laboratory (ARL); Stein et al., 2015), with the Global NOAA NCEP/NCAR reanalysis data files on a latitude–longitude grid of 2.5° , downloaded from the NOAA ARL website (<http://ready.arl.noaa.gov/HYSPLIT.php>). HYSPLIT frequency plots of 96 h AMBTs were constructed for every 6 h during the year 2014 with an arrival altitude of 100 m a.g.l.

3 Results

3.1 Wind occurrence at the MMA

The MMA is highly influenced by easterly anticyclonic air masses that arrive from the Gulf of Mexico, especially during spring and summer (Fig. S5). Figure 2 shows the frequency count of 1 h averages of wind direction by site and season within the MMA during 1993–2014. At all sites, apart from OBI, the predominant wind direction is clearly E, which occurs between 35 and 58 % of the time depending on season. Easterly air masses are augmented by emissions from the industrial area E of the MMA, which are transported across the urban core and prevented from dispersing by the mountains located S-SW of the MMA. On average, the highest wind speeds are observed during summer at all sites. By contrast, calm winds of $\leq 0.36 \text{ km h}^{-1}$ (0.1 m s^{-1}) occurred less than 2 % of the time at all sites, most frequently in winter, and least frequently in summer.

3.2 Time series in O₃ and O_x recorded within the MMA during 1993–2014

Within the MMA, the highest O₃ mixing ratios (1 h averages) are typically observed between April and September, whereas the lowest values are usually recorded between December and January (winter) (Fig. S6). Table S1 summarises the minimum, maximum, average (mean), and median hourly O₃ mixing ratios recorded during 1993–2014. The highest O₃ mixing ratios recorded were 186 ppb at GPE in 1997, 146 ppb at SNN in 2004, and 224 ppb at SNB in 2001. At OBI and STA, the highest O₃ mixing ratios were both recorded on 2 June 1993: 182 ppb at 12:00 CDT at OBI, and 183 ppb at 13:00 CDT at STA, during the occurrence of E winds. Note that all times below are given in CDT. Annual O₃ averages varied from 14 ± 14 ppb at OBI in 2001 to 32 ± 23 ppb at SNB in 1993, whereas O₃ annual medians ranged from 10 ppb at OBI in 2001 to 28 ppb at SNN in 1993.

Reaction with O₃ rapidly converts NO to NO₂, and therefore mixing ratios of odd oxygen ($\text{O}_x = \text{O}_3 + \text{NO}_2$) were calculated to account for O₃ stored as NO₂ for each hour during 1993–2014 at the five sites within the MMA (Table S2; Fig. S7). Minimum values of O_x ranged from 2 ppb, observed at all sites during 1993–2014 to 13 ppb at OBI in 2007. Maxi-

imum values of O_x ranged from 99 ppb at SNN in 2002 to 330 at OBI in 1993. O_x annual averages varied from 23 ± 17 ppb at SNN in 2002 to 51 ± 27 ppb at OBI and at STA in 2001 and 2006, respectively, whereas O_x annual medians ranged from 21 ppb at SNB and SNN, in 2001 and 2002, respectively, to 46 ppb at OBI and STA in 2001 and 2006, respectively. It is clear that the highest O₃ and O_x mixing ratios were recorded when control of precursor emissions of VOCs and NO_x were less stringent than subsequently.

3.3 Diurnal variations in O₃ and O_x within the MMA

Here, O₃ diurnal variations were used to assess changes in the net O₃ production. Figure 3 shows daily profiles by season of O₃, O_x, NO, NO₂, NO_x, and SR averaged over the five sites within the MMA. O₃ generally dips during the morning rush hour due to titration with NO and mirrors the increase in NO₂, which occurs around 07:00 in spring and summer and around 08:00 in autumn and winter. The 1 h difference in the O₃ dip derives from the change to daylight saving time during spring and summer. O₃ generally peaks during the enhanced photochemical period, around 13:00 in spring, 12:00 in summer (coincident with SR), and about 14:00 in autumn and winter. Similar profiles are observed for O₃ in all seasons, being negatively correlated with NO₂ ($r = 0.93$ (winter) to $r = 0.97$ (summer); $p < 0.05$), due to the rapid photolysis of NO₂. Diurnal cycles of O_x behave as O₃, with the lowest values before the morning rush hour and the largest between midday (summer) and 15:00 (winter). During the daytime, O_x and O₃ diurnal cycles are strongly correlated in all seasons, ranging from $r = 0.97$ in winter to $r = 0.99$ in autumn ($p < 0.05$), which suggests net O₃ production during the daytime.

O_x amplitude values (AV_d's) derived from normalised daily cycles were used as a proxy to assess differences in the net O₃ production from site to site within the MMA. The normalised daily cycles were constructed by subtracting daily averages from hourly averages. Figure 4 shows normalised O_x daily cycles. The lowest AV_d's in O_x occur in winter consistent with reduced SR and low photolysis rates, with the largest values observed in summer. It is clear that during the year, the largest AV_d's are recorded at sites downwind of industrial emissions sources, in particular at STA, while the lowest AV_d's are observed at sites upwind. The larger AV_d's at downwind sites are interpreted to indicate higher net O₃ production, derived from the occurrence of photochemical processed air masses from the E sector. The AV_d's at upwind sites are less affected by emissions from the MMA and especially the industrial area.

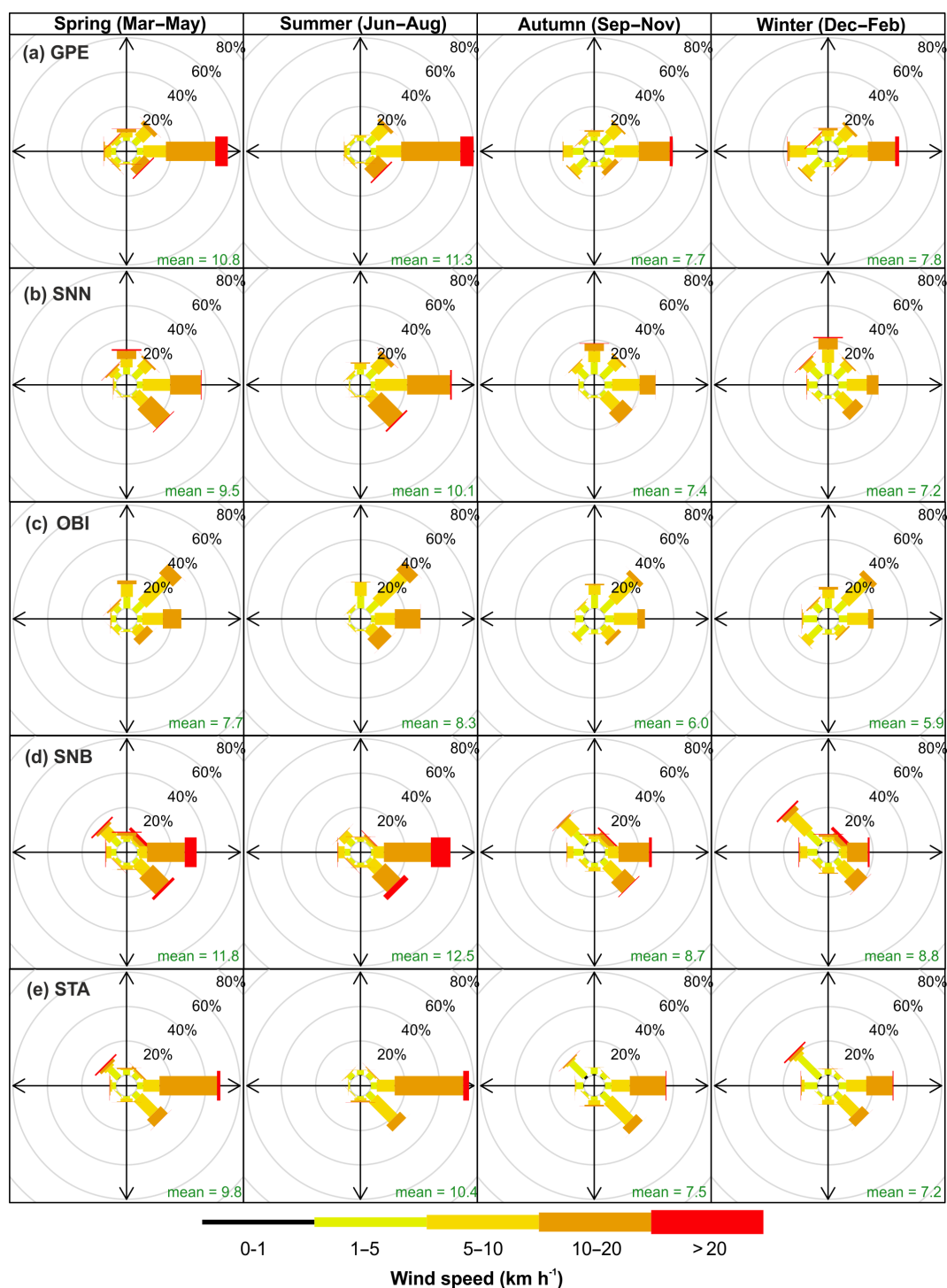


Figure 2. Frequency of counts of measured wind direction occurrence by season and site within the MMA during 1993–2014.

3.4 Annual cycles of O₃ and O_x within the MMA

Annual variations in O₃ and O_x are correlated positively with the seasonality of temperature, RH, and SR (Camalier et al., 2007; Zheng et al., 2007). Annual average cycles for those meteorological variables. O₃ and O_x were constructed by

averaging monthly averages for the same month during the studied period. Figure 5a shows that O₃ exhibits the maxima during spring and minima in winter, with a downward peak in early autumn, a behavioural characteristic of tropospheric O₃ in the NH. O_x peaks in spring and dips in summer; although it is evident that NO_x emissions lead to apparently similar O_x

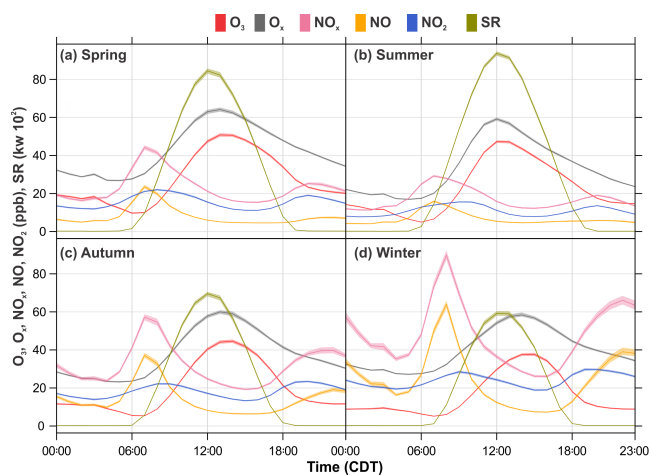


Figure 3. Seasonal average daily profiles for O₃, O_x, NO_x, NO, NO₂, and SR within the MMA during 1993–2014. The shading shows the 95 % confidence intervals of the average.

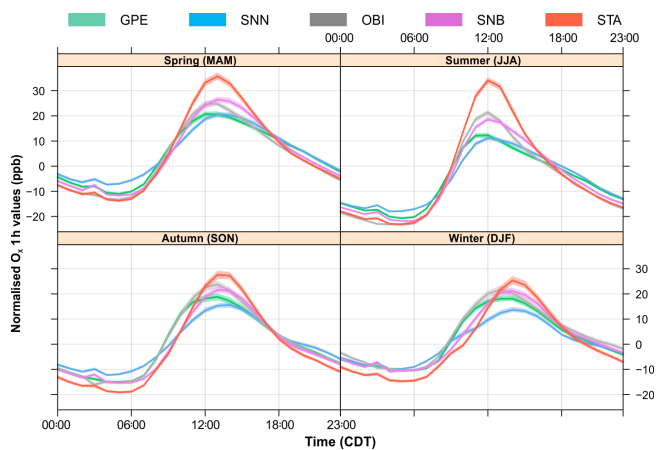


Figure 4. Seasonal O_x de-trended daily profiles within the MMA during 1993–2014. De-trended O_x daily cycles were constructed by subtracting daily averages from hourly averages to remove the impact of long-term trends.

levels in winter and spring despite the decrease in O₃ levels. A correlation analysis among monthly averages for both O₃ and O_x with temperature, rainfall, RH, and SR revealed that the strongest relationship was between O₃ and SR ($r = 0.72$, $p < 0.001$; Fig. 5a), with a relationship evident with O_x.

The seasonal amplitude value (AV_s) provide insight into inter-annual variations in net O₃ production in response to changes in precursor emissions, meteorology, and O₃ chemistry. The seasonal cycles in O₃ during 1993–2014 were determined by filtering monthly averages with the STL technique (Cleveland et al., 1990) (Fig. S8). O₃ AV_ss were calculated as the difference from peak to trough (spring peak). An average O₃ AV_s of 15.1 ± 2.97 (1σ) ppb was calculated from 1993 to 2014 within the MMA, with the lowest O₃ AV_s of 10.3 ppb determined in 1998, and the largest

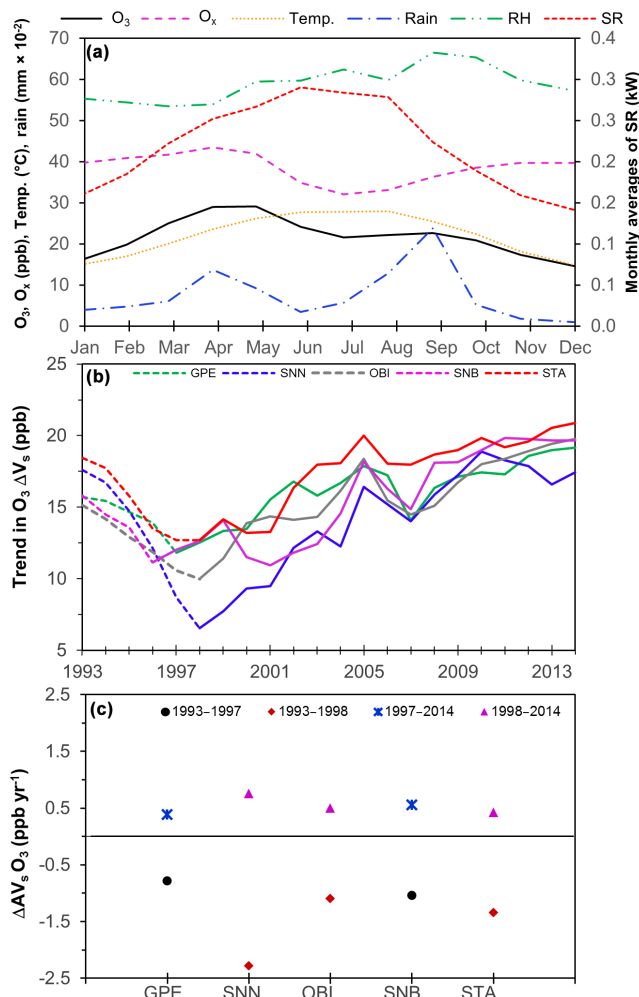


Figure 5. (a) Annual cycles of O₃, temperature, rainfall, RH, and SR constructed by averaging records from 1993 to 2014 for a 1-year period. (b) Trends in AV_s of O₃ recorded at the five monitoring sites within the MMA from 1993 to 2014. The decline in AV_s observed is due to the economic crisis experienced in Mexico during 1994–1996, followed by persistent increases in AV_s since 1998. (c) Annual rates of change in O₃ AV_s by site before and after the 1994–1996 economic crisis.

O₃ AV_s of 19.0 ppb observed in 2014. Figure 5b shows that O₃ AV_s decreased significantly at all sites between 1993 and 1997–1998, at rates from 0.78 ppb O₃ yr⁻¹ at GPE to 2.28 ppb O₃ yr⁻¹ at SNN (Fig. 5c). O₃ AV_s's have increased constantly ($p < 0.05$) at all sites since 1998, ranging from 0.90 ppb O₃ yr⁻¹ at GPE to 0.75 ppb O₃ yr⁻¹ at SNN. O_x AV_ss exhibited no discernible trends at all sites for the whole studied period, although SNN showed a significant ($p < 0.05$) decline during 1993–2001 (1.5 ppb yr⁻¹) and STA showed an increase during 2004–2010 (1.3 ppb yr⁻¹). The trends in O_x follow those observed for NO_x at SNN and STA during 1993–2014, which indicates that nearby indus-

trial emissions have a significant contribution to the observed O_x levels within the MMA.

3.5 Long-term trends in O₃ and O_x within the MMA during 1993–2014

Quantifying the absolute changes in ground-level O₃ in response to trends in its precursor emissions is crucial to evaluate the impacts of air quality control (Parrish et al., 2009; Simon et al., 2015). The growing economy within the MMA has increased O₃ precursor emissions from point and area sources due to the limited emissions control programs (INEGI, 2015; SDS, 2015). Moreover, predominant E-SE winds throughout the year transport primary pollutants and their oxidised products downwind from the industrial area, which can offset reductions in emissions from other sources. Here, to characterise changes in net O₃ production during 1993–2014 within the MMA in response to changes in its precursor emissions, long-term trends for daytime (06:00–18:00 CDT) O₃ and O_x measurements were derived by averaging data in seasonal periods. Seasonal averaging was used to minimise variability inherent in longer-term averages and the de-seasonalisation process avoids confounding overall trends, especially when seasons exhibit opposite trends (Parrish et al., 2009).

Figure 6 shows seasonal trends in O₃ within the MMA, and Table 3 summarises the parameterisation of the trends. Significant increases ($p < 0.1$) in O₃ are observed at all sites, apart from STA, in spring and summer, while in autumn, O₃ increases significantly only at SNN and SNB. The increases in O₃ range from 0.26 ppb yr⁻¹ in spring at OBI to 0.47 ppb yr⁻¹ in summer at SNN. Overall, the lowest O₃ growth rates are observed at the urban background GPE site, whereas the largest ones are at the industrial SNN site. It is worth noting that only SNN and OBI exhibit significant increases in autumn, despite a decrease in the frequency of high wind speeds ($> 20 \text{ km h}^{-1}$). The existence of significant trends at all sites during spring–summer, except for OBI, is consistent with the downwind transport of industrial emissions and the high frequency of photochemical processed air masses with NE-E-SE origin, where the industrial area is located (Fig. S9).

Seasonal trends in O_x are shown in Fig. 7, with the parameters of the trends listed in Table 3. Consistent with the seasonal O₃ trends observed, significant increases ($p < 0.1$) in O_x within the MMA are determined in spring at all sites except for STA and range from 0.02 ppb yr⁻¹ at OBI to 0.67 ppb yr⁻¹ at SNB. It is worth noting that the industrial SNN and SNB sites show significant increases in O_x in all seasons, with the lowest growth rates in winter and the largest in summer and spring. Moreover, STA exhibits the only significant decrease in O_x of 0.63 ppb yr⁻¹ during winter. As for O₃, the O_x increasing trends are consistent with the transport of primary emissions during the high occurrence of NE-E-SE air masses at $WS > 10 \text{ km h}^{-1}$, which is highlighted during

the photochemical season (April–September). Furthermore, the small shift in wind direction at STA to NW during winter coincides with the only observed decrease in net O₃ production within the MMA, which confirms that O₃ precursors are emitted E of the MMA. This also makes evident that increasing upwind industrial emissions have offset reductions in emissions from on-road sources as revealed by the decline in NO_x evident at OBI.

3.6 Comparison of MMA O₃ and O_x weekly profiles with those in MCMA and GMA

O₃ production varies from city to city in response to local NO_x and VOC emissions. Assessment of weekly profiles of O₃ and O_x may provide insights into the geographic response in net O₃ production to diurnal variations in precursor emissions. Hourly O₃ and O_x averages were used to construct weekday and weekend average profiles for the MCMA from 1993 to 2014, and for the GMA from 1996 to 2014. Figure 8 compares weekly O₃ and O_x profiles by season within the MMA with those for the MCMA and GMA. In each case, and consistent with observations in other major urban areas of NA, the lowest O₃ mixing ratios occur during the morning rush hour due to O₃ titration with NO emitted from on-road sources, whereas peak values of O₃ are apparent after midday during periods of enhanced SR (Stephens et al., 2008; Jaimes-Palomera et al., 2016). It should be noted that the peak value of O₃ for the GMA in winter and spring occurs an hour or so earlier than for the MMA and MCMA, which is consistent with higher VOC/NO_x emissions ratios in the GMA (Kanda et al., 2016). As might be anticipated, larger AV_d's of $76.9 \pm 1.6 \text{ ppb O}_3$ are observed for the MCMA than for the GMA ($46.1 \pm 1.0 \text{ ppb O}_3$) and MMA ($37.6 \pm 0.4 \text{ ppb O}_3$), related to the levels of emissions of the O₃ precursors. The O_x profiles show a trough during the morning rush hour and a peak between 12:00 and 14:00 in all urban areas. Despite large variations between weekday and weekend NO_x mixing ratios in the three urban areas as shown in Fig. 8, no significant differences ($p > 0.05$) in O₃ and O_x are observed in any of the metropolitan areas between O₃ and O_x weekend and weekday AV_d's.

Stephens et al. (2008) suggested that the most plausible explanation for the lack of weekend O₃ effect at MCMA during 1987–2007 is a simultaneous decrease in NO_x and VOC emissions on weekends since the sole decrease in NO_x emissions under VOC-limited conditions would lead to an increase in O₃ not observed. Similarly, a VOC-limited O₃ production regime was reported for the MMA by Sierra et al. (2013), whereas Kanda et al. (2016) reported that in the GMA the O₃ production lies in the region between VOC and NO_x sensitivity. Therefore, it can be suggested that simultaneous decreases in NO_x and VOC emissions on weekends in the GMA and MMA explain the similar behaviour in O₃ and O_x in the MCMA. Moreover, a change in NO_x-limited O₃ production regime on weekends in the three urban areas

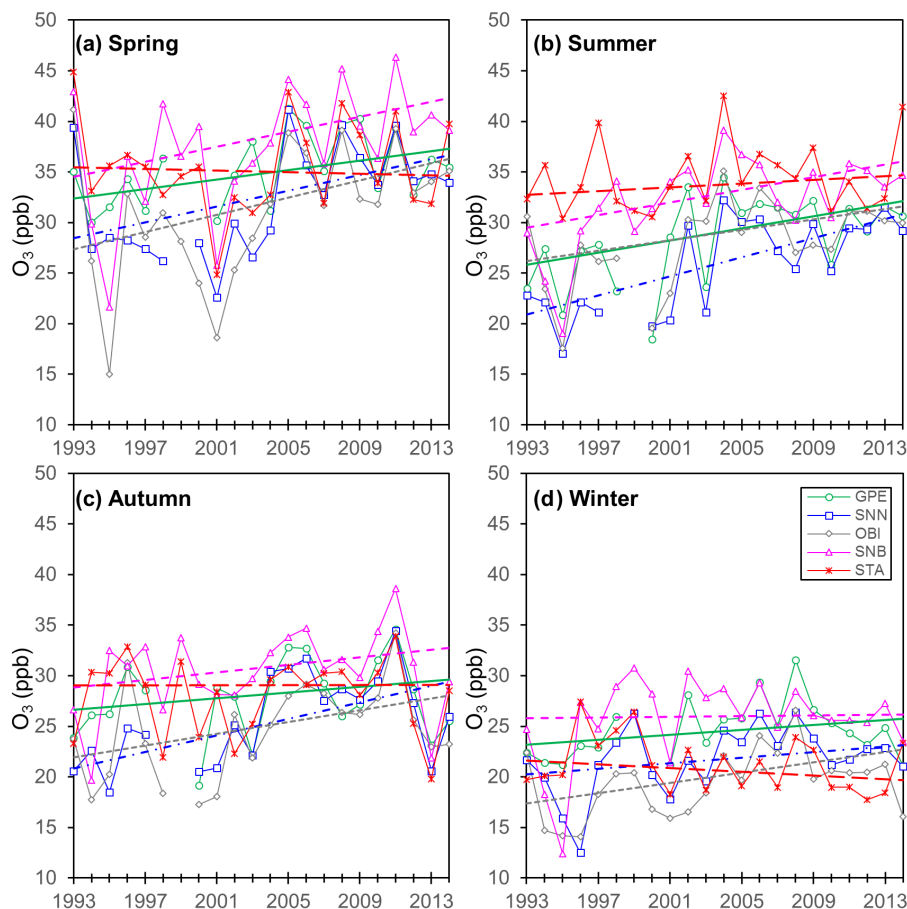


Figure 6. Seasonal trends in O₃ within the MMA during 1993–2014. Each data point represents the average of the 3-month period that defines the season. The continuous lines show the Sen trend.

seems unlikely since this would result in lower O₃ levels on weekends, which is not observed in any of the studied urban areas (Torres-Jardon et al., 2009). Wolff et al. (2013) observed similar O₃ levels during weekdays and on weekends in several urban areas in the US despite lower O₃ precursor emissions over weekends. Furthermore, the number of sites in the US that exhibited a weekend effect decreased from ca. 35 % to less than 5 % from 1997–1999 to 2008–2010, which was attributed to an increase in the VOC/NO_x emissions ratio derived from a greater decline in NO_x than in VOC emissions, mostly driven by reductions from on-road sources.

3.7 Long-term trends in MCMA, GMA, and MMA from 1993 to 2014

The high mixing ratios of O₃ typically observed at the three largest urban areas in Mexico have motivated the introduction of control strategies to decrease emissions of the O₃ precursors, NO_x and VOCs. The success of the control strategies implemented can be evaluated by assessing trends in O₃ and O_x. As for the MMA, seasonal trends in O₃ and O_x within the MCMA and GMA were calculated from daytime measure-

ments. Figure 9 shows a comparison of inter-annual trends in O₃ and O_x in the three urban areas in Mexico, and Table 4 lists the parameters of the trends. Overall, during 1993–2014, daytime O₃ in the MCMA decreased significantly ($p < 0.05$) by 1.15 ppb yr⁻¹ (2.04 % yr⁻¹) and increased in the MMA by 0.22 ppb yr⁻¹ (0.84 % yr⁻¹); in the GMA no discernible trend was observed during 1996–2014. For daytime O_x in the MCMA and GMA during the same periods, significant decreases ($p < 0.05$) of 1.87 and 1.46 ppb yr⁻¹, respectively, were determined, while the MMA did not exhibit a significant change. At the MCMA, the overall trends in O₃ and O_x are strongly driven by their wintertime decreases of 1.62 and 2.47 ppb yr⁻¹, respectively, whereas in the MMA, the annual growth in O₃ is driven by increases in spring and summer of 0.32 and 0.27 ppb yr⁻¹, respectively. However, in the MMA, an increase in O_x of 0.28 ppb yr⁻¹ is observed only during summer. The overall O_x trend is strongly affected by the non-significant trends in the other seasons. It is worth noting that in the GMA, the overall decrease in O_x of 1.46 ppb yr⁻¹ is similar for all seasons, which range between 1.40 ppb yr⁻¹ (autumn) and 1.89 ppb yr⁻¹ (spring).

Table 3. Results for O₃ and O_x long-term trends expressed in ppb yr⁻¹ for 1993–2014 at the five sites within the MMA by season.

Site	Period	Ozone (O ₃)			Odd oxygen (O _x = O ₃ + NO ₂)		
		ppbyr ⁻¹	% yr ⁻¹	Significance	ppbyr ⁻¹	% yr ⁻¹	Significance
GPE	Annual	0.21	0.78	b	0.31	0.80	c
	Spring	0.24	0.73	b	0.32	0.69	b
	Summer	0.30	1.16	b	0.38	1.18	b
	Autumn	0.14	0.53		0.25	0.62	
	Winter	0.12	0.53		0.14	0.33	b
SNN	Annual	0.33	1.40	d	0.45	1.25	b
	Spring	0.39	1.38	b	0.49	1.22	b
	Summer	0.47	2.24	b	0.58	1.87	d
	Autumn	0.41	1.96	b	0.65	1.94	b
	Winter	0.14	0.68		0.23	0.58	a
OBI	Annual	0.30	1.29	b	-0.17	-0.35	
	Spring	0.43	1.56	b	0.02	0.03	b
	Summer	0.26	0.98	b	-0.04	-0.09	
	Autumn	0.29	1.33	a	-0.66	-1.15	
	Winter	0.25	1.46		-0.28	-0.53	
SNB	Annual	0.19	0.65	a	0.61	1.66	c
	Spring	0.37	1.07	a	0.67	1.65	a
	Summer	0.31	1.06	d	0.66	2.17	d
	Autumn	0.19	0.64		0.60	1.61	a
	Winter	0.02	0.07		0.47	1.12	a
STA	Annual	0.01	0.01		-0.15	-0.28	
	Spring	-0.04	-0.11		-0.01	-0.02	
	Summer	0.09	0.28		0.13	0.27	
	Autumn	0.00	0.00		-0.22	-0.41	
	Winter	-0.09	-0.43		-0.63	-1.15	b

^a Level of significance $p < 0.1$. ^b Level of significance $p < 0.05$. ^c Level of significance $p < 0.001$. ^d Level of significance $p < 0.001$.

The overall trends in net O₃ production during 1993–2014 in the MCMA and GMA are consistent with the significant ($p < 0.05$) annual decreases in NO_x of 1.21 and 1.25 ppbyr⁻¹, respectively (Fig. 10). By contrast, while average NO_x levels have increased annually in the MMA at the rate of 0.33 ppbyr⁻¹ ($p < 0.05$), the average net O₃ production has remain steady. It is possible that the non-linear response in O_x to the changes in NO_x in an environment of high NO_x mixing ratios (> 60 ppb) displaces the chemical equilibrium to favour NO as the dominant component of NO_x, which does not account for the levels of O_x (Clapp and Jenkin, 2001). It is also possible that the O_x trends derived from the combined data set for the MMA do not represent local observed trends because there is a compensating effect between O_x reductions and increases.

3.8 Compliance with the 1 and 8 h Mexican standards for O₃ within the MMA

Between 1993 and 2014, there were two official standards for maximum permitted mixing ratios of O₃ in Mexico: (i) a running 8 h average of 80 ppb, not to be exceeded more than four times per calendar year, and (ii) a 1 h average of 110 ppb (NOM-020-SSA1–1993). Since 19 October 2014, the maximum permitted O₃ levels were lowered to a running 8 h average of 70 ppb and a 1 h average of 95 ppb, (NOM-020-SSA1-2014). However, because both standards are applicable for whole calendar years, the old permitted O₃ levels were used in this study to determine the number of annual exceedances of both O₃ standards. Figure 11 shows that within the MMA, the O₃ 1 h average and the running 8 h standards were frequently exceeded (INE, 2011; SEMARNAT, 2015). The largest number of exceedances occurs at STA, followed by SNB, GPE, and OBI, whereas the fewest breaches have been observed at SNN markedly since 2004. However, there have been three periods of clear decreased exceedances at all

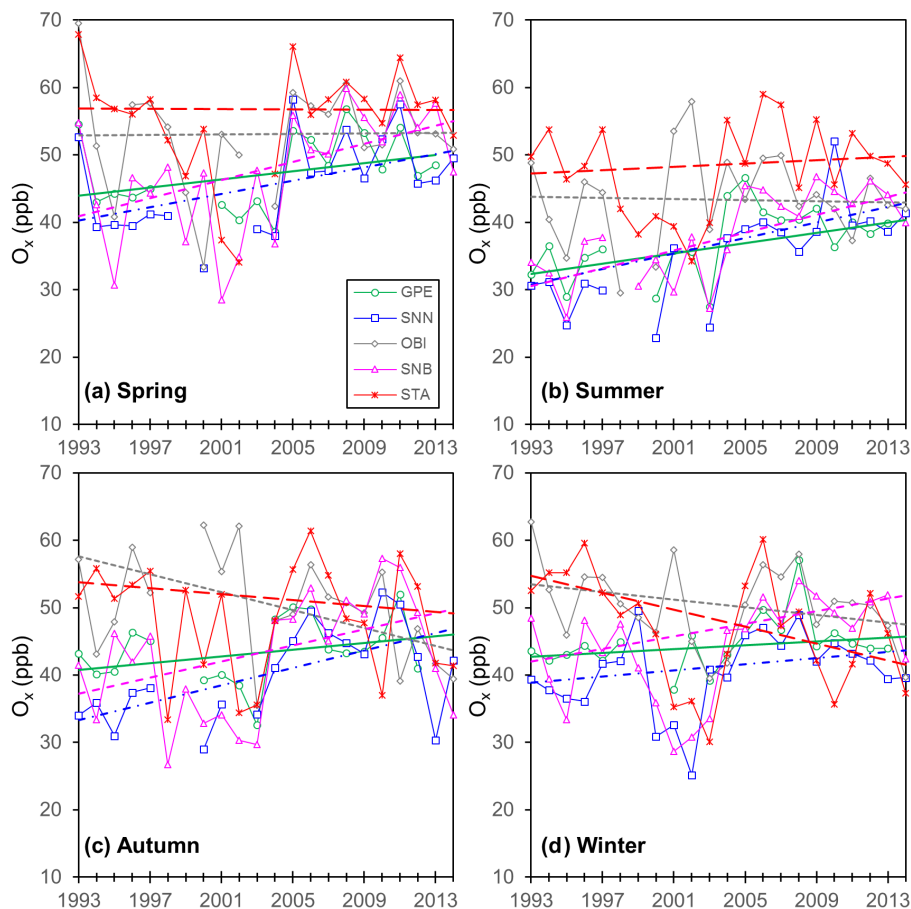


Figure 7. Seasonal trends in O_x within the MMA during 1993–2014. Each data point represents the average of the 3-month period that defines the season. The continuous lines show the Sen trend.

sites (except STA in 2014) during 1994–1995, 1999–2000, and 2012–2013, which are consistent with marked changes in the national GDP during economic recessions in Mexico (Fig. S10a). However, national GDP exhibits a notable decrease during the 2008–2009 global economic recession; only in 2009 do the O₃ annual exceedances within the MMA seem to follow (Fig. S10b).

Therefore, if O₃ levels continue to increase within the MMA, as determined in the long-term trend assessment, an increase in peak O₃ mixing ratios is also likely to occur. Hence, to analyse changes in peak O₃, daily maxima 1 h averages from 1993 to 2014 were used to determine seasonal trends in peak levels. Figure 12 shows trends in 1 h daily maxima and Table 5 lists the parameters of the trends. Daily maxima O₃ 1 h averages increased significantly ($p < 0.05$) in spring and summer at all sites, except for STA, and also in autumn at the industrial sites SNN and SNB. The largest increases in the daily maxima are seen at SNN, where similar increases between 0.85 and 0.93 ppbyr⁻¹ are determined between spring and autumn. SNB exhibits slightly lower growth rates in spring and summer but a large difference in autumn. We have shown that predominantly E-

SE winds transport photochemically processed air masses to SNN and SNB during spring–summer leading to the observed exceedances. Moreover, the change in the wind occurrence in autumn at SNB leads to a lower growth rate than at SNN, where the calmest winds during the whole year drive the largest increase, interpreted to be due to the photochemical processing of precursors emitted locally. The GPE and OBI sites exhibit increases only in spring and summer, with the lowest increases of all sites of 0.48 ppbyr⁻¹ determined at OBI in spring, which contrasts with the largest increase at OBI during the same season. However, such increases are consistent with an increase in the occurrence of NE and E air masses at high speeds ($> 10 \text{ km h}^{-1}$) during spring–summer. STA shows a significant decrease in the maximum daily O₃ 1 h averages of 0.35 ppbyr⁻¹ in winter, which is consistent with an increase in the occurrence of NW air masses at WS $< 5 \text{ km h}^{-1}$, loaded with high NO_x mixing ratios (50 ppb) that promote the O₃ titration.

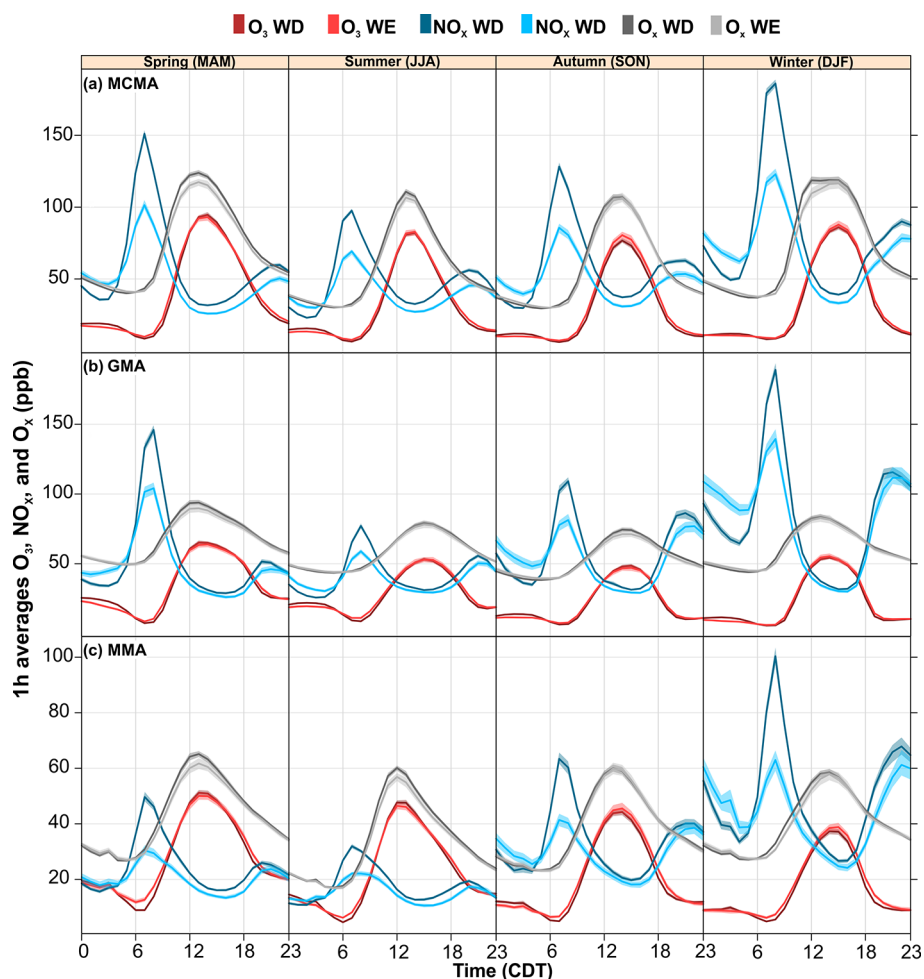


Figure 8. Seasonal average diurnal cycles of O₃, O_x, and NO_x during 1993–2014 for the MCMA and the MMA, and between 1996 and 2014 for the GMA. The shading shows the 95 % confidence intervals of the average, calculated through bootstrap resampling (Carslaw, 2015).

4 Discussion

4.1 Strategies for air quality control in Mexico

The Mexican environmental authorities have focused largely on improving the air quality within the MCMA since 1986 by implementing numerous strategies to control primary emissions, but they have paid less attention to other large metropolitan areas in Mexico (PICCA, 1990; ProAire-MCMA, 2011). Control measures have been designed based on NAEI and local emissions inventory data, which possess significant uncertainties (Arriaga-Colina et al., 2004; Velasco et al., 2007; Kanda et al., 2016). However, despite these uncertainties, the emissions control strategies have helped to reduce O₃ levels within the MCMA since 1991–1992 (ProAire-MCMA, 2001). Here, we describe the most effective measures introduced to control O₃ precursor emissions within the MCMA, and then we discuss potential benefits of implementing such measures within the MMA.

From 1993 to 2014, NO_x levels within the MCMA decreased at a rate of around 1.2 ppb yr⁻¹ (1.6 % yr⁻¹) as determined from ground-based measurements. This decline is remarkably consistent with the decrease in the NO₂ column over the MCMA of 1.6 % yr⁻¹ during 2005–2014 reported by Duncan et al. (2016). The decrease in NO_x was driven largely by reductions in emissions from on-road sources, in response to the introduction of mandatory three-way catalytic converters in new vehicles in 1993 (NOM-042; SEMARNAT, 1993b) and by the introduction of a no-driving day and more stringent exhaust emissions inspection programs for private cars in 1989 (NOM-041; SEMARNAT, 1993a). The NO_x reduction measures also required public transport vehicles to switch from engines fuelled by petrol to engines fuelled by LP gas. New road corridors were designed for improving the intracity transport and the public transport fleet was renewed (ProAire-MCMA, 2001). For industrial sources, the switch from fuel oil to LP gas fuel, relocation of highly polluting industries away from the MCMA, and im-

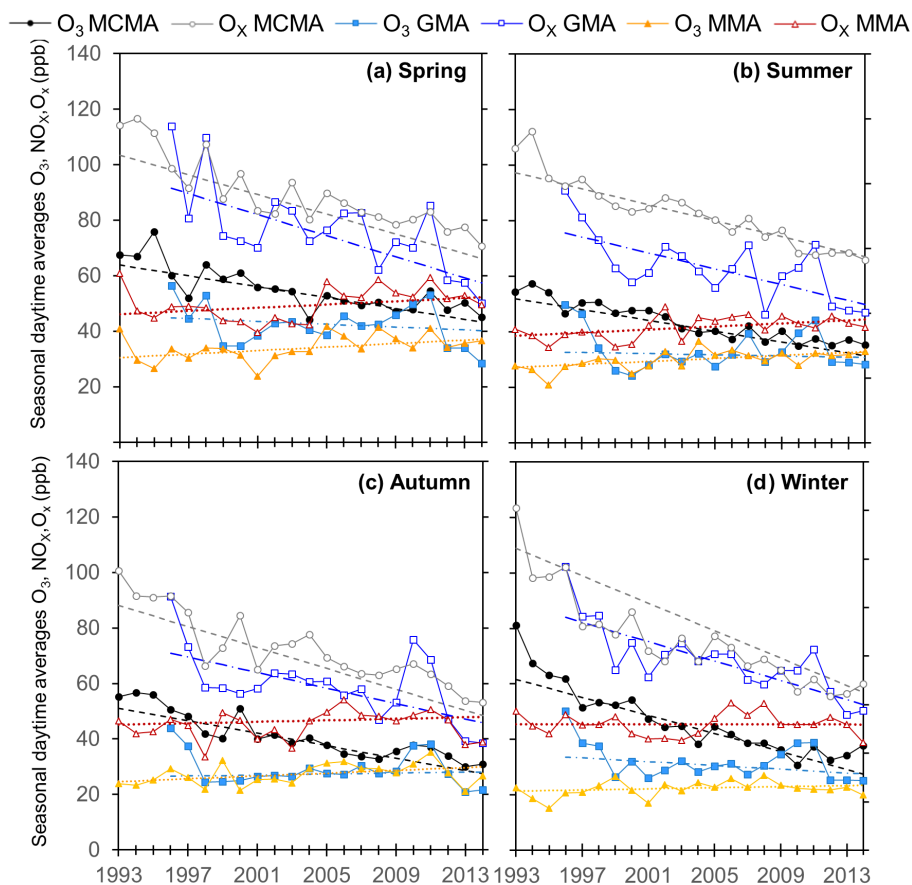


Figure 9. Seasonal trends in O₃ and O_x for the MCMA and MMA during 1993–2014 and for the GMA during 1996–2014. Each data point represents the average of the 3-month period that defines the season. The dashed lines show the Sen trend.

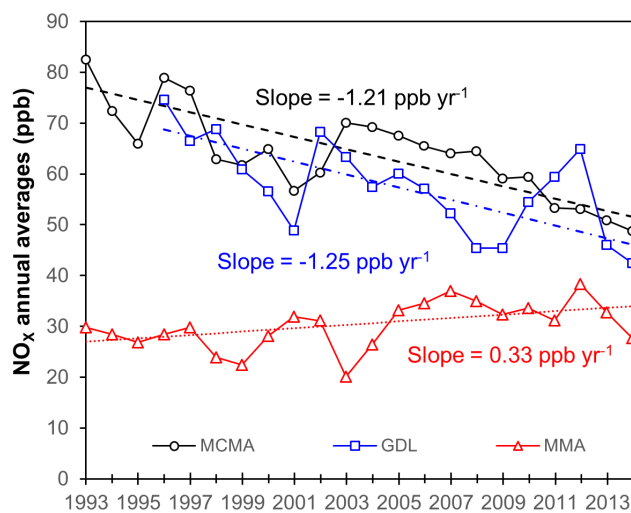


Figure 10. Trends in NO_x in the MCMA and MMA during 1993–2014 and in the GMA during 1996–2014. The dashed lines represent the Sen slopes. All trends are statistically significant at $p < 0.05$.

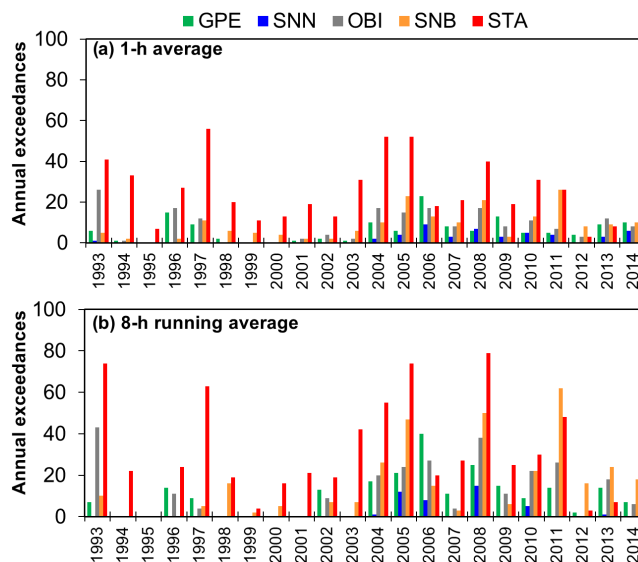


Figure 11. Annual exceedances of the O₃ NOM for 1 h averages (110 ppb) and 8 h running averages (80 ppb) at the five monitoring sites within the MMA from 1993 to 2014.

Table 4. Results for O₃ and O_x long-term trends by season expressed in ppb yr⁻¹ during 1993–2014 for the MCMA and MMA and during 1996–2014 for the GMA.

Urban area	Period	Ozone (O ₃)			Odd oxygen (O ₃ + NO ₂)		
		ppb yr ⁻¹	% yr ⁻¹	Significance	ppb yr ⁻¹	% yr ⁻¹	Significance
MCMA	Annual	-1.15	-2.04	d	-1.87	-1.94	d
	Spring	-0.97	-1.53	d	-1.77	-1.71	d
	Summer	-0.97	-1.88	d	-1.44	-1.67	d
	Autumn	-1.12	-2.20	d	-1.89	-2.15	d
	Winter	-1.62	-2.64	d	-2.47	-2.27	d
GMA	Annual	-0.29	-0.81		-1.46	-1.85	+
	Spring	-0.26	-0.57		-1.89	-2.07	b
	Summer	-0.10	-0.32		-1.43	-1.89	b
	Autumn	-0.09	0.33		-1.40	-1.97	b
	Winter	-0.34	-1.01		-1.74	-2.08	d
MMA	Annual	0.22	0.84	c	0.13	0.30	
	Spring	0.32	1.04	c	0.29	0.63	
	Summer	0.27	0.99	d	0.28	0.72	d
	Autumn	0.25	1.03		0.13	0.31	
	Winter	0.10	0.45		0.01	-0.01	

^a Level of significance $p < 0.1$. ^b Level of significance $p < 0.05$. ^c Level of significance $p < 0.001$. ^d Level of significance $p < 0.001$.

plementation of regular inspection programs of NO_x emission for industrial and area sources were also implemented (ProAire-MCMA, 2001).

While the outlook for NO_x levels within the MCMA is clear, studies of VOC levels have reported no conclusive trends. For instance, Arriaga-Colina et al. (2004) reported a decrease in VOCs of around 10 % from 1992 to 2001 over the N MCMA, while Garzón et al. (2015) reported that on average VOCs increased over most of the MCMA between 1992 and 2002 but decreased by 2.4 ppb yr⁻¹ between 2002 and 2012. However, the decrease in VOCs from 2002 to 2012 reported by Garzón et al. (2015) is consistent with a reduction in light alkane and aromatic levels during the morning rush hour reported by Jaimes-Palomera et al. (2016). Continuous measurements of VOCs have been recently introduced by the MCMA government, which precludes an assessment of VOC long-term trends. The measures implemented to control VOC emissions from on-road sources have included the reformulation of petrol with the reduction of highly reactive VOCs and addition of oxygenated compounds and fitting of three-way catalytic converters in all new vehicles (NOM-042; SEMARNAT, 1993b; ProAire-MCMA, 2001). For area sources, control measures include the introduction of vapour emissions control systems at petrol stations and the introduction of a LP gas leak detection program for the distribution network (ProAire-MCMA, 2011). As for NO_x, industrial VOC emissions sources have been subject to regular emissions inspections and relocation of the most significant emitters (ProAire-MCMA, 2011).

Therefore, the moderate success on controlling O₃ levels within the MMA can be interpreted as due to the implementation of effective control measures on VOCs and NO_x emissions. Thus, a comparison between VOCs and NO_x trends derived from the NAEI and local emissions inventories with those determined from ground-level measurements can provide insight into further improvements in decreasing O₃ levels not only within the MCMA but also in other large metropolitan areas in Mexico. Within the MCMA, the NAEI NO_x emissions trends are consistent with the decrease determined from ground-based measurements made by SIMAT, but the MCMA local inventory trends disagree with the SIMAT trends (Figs. S1 and 10). For VOCs, the NAEI and the MCMA inventories oppose measured trends in VOCs during 1993–2001 (Arriaga-Colina et al., 2004; Garzón et al., 2015). This can be explained by underestimates of VOC emissions within the MCMA of a factor of 2–3 (Arriaga-Colina et al., 2004; Velasco et al., 2007). Such discrepancies suggest that significant improvements in NO_x and VOC emissions inventories are still required to better inform O₃ control strategies.

4.2 Ground-level O₃ and O_x variations within the MMA

The O₃ and O_x diurnal variations result from the particular chemical environment and meteorological conditions at each monitoring site within the MMA. Thus, the largest O₃ and O_x mixing ratios, except for OBI, are typically observed for air masses from the E and SE wind sectors, whereas at

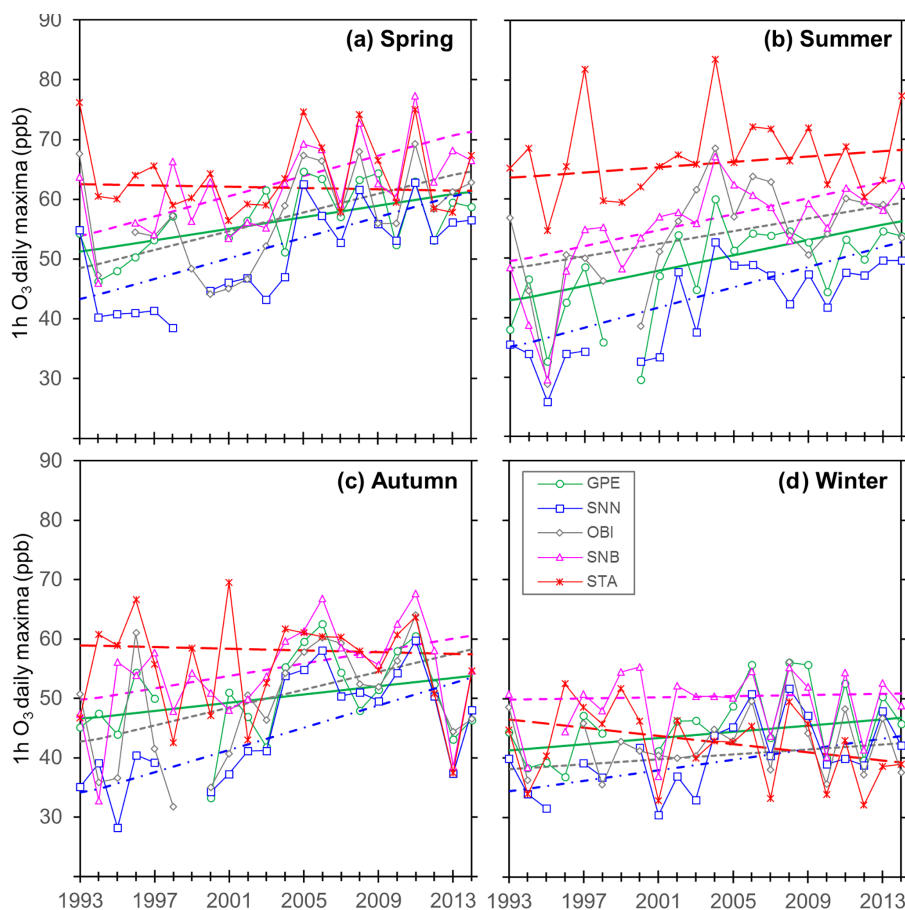


Figure 12. Seasonal trends in 1 h O₃ daily maxima at the MMA during 1993–2014. Each data point represents the average of the 3-month period that defines the season. The dashed lines show the Sen trend.

OBI, the largest O₃ and O_x values are recorded during the occurrence of NE and E air masses. It is clear that short-range transport and large upwind emissions of O₃ precursors from the industrial area dominate the MMA (SEMARNAT, 2006, 2011, 2014; SDS, 2015). This is underlined at OBI with the highest values of O_x where the predominant wind direction is NE, consistent with the transport of emissions from the industrial area located to the NE and photochemical processing of air masses (Carrillo-Torres et al., 2017). The daily cycles of O₃ determined within the MMA are consistent with those reported for Los Angeles (VanCuren, 2015) and Toronto (Pugliese et al., 2014). In Toronto, the O₃ maxima were enhanced by the arrival of photochemically processed air masses transported from polluted wind sectors, and decreased during clear air masses. This behaviour is similar to that observed within the MCMA, with enhanced O₃ maxima during the occurrence of E-SE (polluted) air masses and decreased levels when W-SW (relatively clean) air masses occurred.

4.3 Origin of the O₃ annual cycles within the MMA

The annual O₃ cycles within the MCMA are consistent with the spring maxima and winter minima characteristic of the southeastern US regions (Strode et al., 2015) and follow the O₃ cyclic pattern at NH mid-latitudes (Monks, 2000; Vingarzan, 2004). However, they are different from O₃ annual cycles reported for the US west coast regions, particularly in California, where the maxima in the cycle occurs between June and August, driven by the local influence of precursor emissions on O₃ production and photochemical conditions (Vingarzan, 2004; Strode et al., 2015). The recurrent downward spikes in the O₃ annual cycles within the MMA between July and August result from high wind speeds (> 10 km h⁻¹ on average) that disperse O₃ precursors and increase the boundary layer height (ProAire-MMA, 2008). The peak in O₃ observed in September is characteristic of humid regions and can be ascribed to an increase in OH radicals derived from the increment in RH during the rainy season (Lee et al., 2014). A marked increase in RH within the MMA during September is consistent with the increase in O₃ observed as reported by Lee et al. (2014). Over the Midwestern and

Table 5. Results for O₃ daily maximum long-term trends by season in ppb yr⁻¹ during 1993–2014 at the five sites within the MMA.

Site	Period	Ozone (O ₃)		Significance
		ppb yr ⁻¹	% yr ⁻¹	
GPE	Annual	0.45	1.02	c
	Spring	0.48	0.94	c
	Summer	0.64	1.50	b
	Autumn	0.35	0.74	
	Winter	0.26	0.63	
SNN	Annual	0.79	2.13	d
	Spring	0.87	2.01	d
	Summer	0.85	2.42	d
	Autumn	0.93	2.73	b
	Winter	0.44	1.29	
OBI	Annual	0.65	1.51	b
	Spring	0.78	1.62	c
	Summer	0.53	1.10	b
	Autumn	0.75	1.77	
	Winter	0.21	0.55	
SNB	Annual	0.40	0.80	d
	Spring	0.85	1.58	d
	Summer	0.67	1.36	d
	Autumn	0.52	1.05	b
	Winter	0.05	0.10	
STA	Annual	0.01	-0.01	
	Spring	-0.05	-0.09	
	Summer	0.22	0.35	
	Autumn	-0.07	-0.12	
	Winter	-0.35	-0.75	a

^a Level of significance $p < 0.1$. ^b Level of significance $p < 0.05$. ^c Level of significance $p < 0.001$. ^d Level of significance $p < 0.001$.

eastern US regions, that O₃ peak has become less noticeable since 2000 (Zheng et al., 2007).

The annual variability in O₃ within the MMA is strongly coupled to the economic conditions (GDP) in Mexico. For instance, the economic crisis of 1994–1996 caused a marked reduction in industrial emissions of VOCs and NO_x, which is confirmed by the significant decrease in O₃ annual variations at all sites within the MMA (Tiwari et al., 2014; INEGI, 2016). During the global economic recession of 2008–2009, Castellanos and Boersma (2012) reported a reduction of 10–30 % in tropospheric NO₂ over large urban European areas, which is consistent with a faster decline of $8 \pm 5 \text{ % yr}^{-1}$ in the NO₂ column density during the same period for US urban regions (Russell et al., 2012). Increases in the NO₂ column density over the MMA as reported by Duncan et al. (2016) are explained by the gradual recovery of the economy since 1997 in Mexico. Moreover, increases in O₃ precursor emissions and in annual variability observed within the MMA are consistent with such economic growth. This clearly ex-

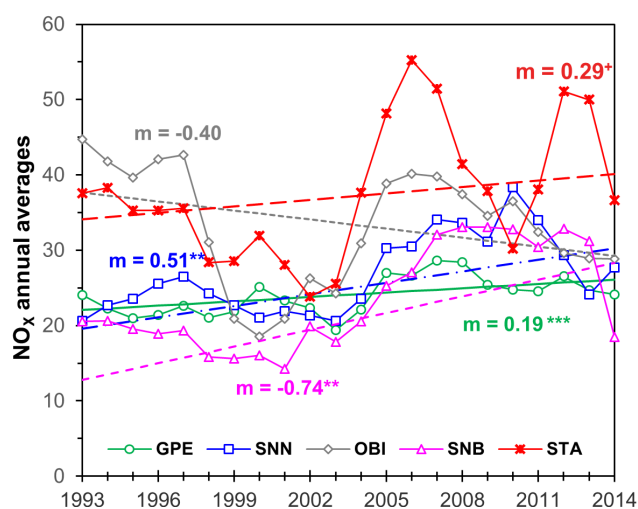


Figure 13. Long-term trends for NO_x at the five monitoring sites within the MMA during 1993–2014. The dashed lines represent the Sen slopes. Annual NO_x rates of change are expressed as the slope (m) of the dashed lines in units of ppb yr⁻¹. Levels of confidence are represented as ⁺ = $p < 0.1$, * = $p < 0.05$, ** = $p < 0.001$, and *** = $p < 0.001$.

plains the opposite trends in O₃ annual variations before and after the economic crisis within the MMA, with the lowest changes seen at the urban GPE site and the greatest ones detected for the SNN industrial site.

4.4 Increasing O₃ and O_x levels within the MMA

Ground-based measurements made during 1993–2014 reveal significant ($p < 0.05$) increases in NO_x within the MMA at all sites, apart from OBI, which exhibits a significant decrease (Fig. 13). Overall, the NO_x increase within the MMA of 1.24 % yr^{-1} (0.33 ppb yr^{-1}) during 1993–2014 is larger than the increase in the NO₂ column density over the MMA of around 0.78 % yr^{-1} during 2005–2014 reported by Duncan et al. (2016); although both have indicated a significant increase in the NO_x levels at least since 2005. The largest increases in NO_x correspond to industrial sites SNN (0.51 ppb yr^{-1}) and SNB (0.74 ppb yr^{-1}). This is interpreted as a response to growing industrial activity, in combination with flexible emissions regulations within the MMA (INEGI, 2016). The influence of industrial emissions upon O₃ at the MMA becomes evident from the lowest NO_x growth rate of 0.19 ppb yr^{-1} observed at GPE since OBI has few occurrences of air masses transporting pollutants from the largely industrialised areas throughout the year (Fig. 2). By contrast, the NO_x decrease of $-0.40 \text{ ppb yr}^{-1}$ at OBI arises from decreases in emissions from on-road sources (SDS, 2015). The large growth rates in O₃ and NO_x at SNN and SNB are explained by increasing emissions of O₃ precursors from a growing number of industries and the urban development E of the MMA. The most likely explanation for the O₃ in-

crease at OBI is a reduced titration effect from decreasing NO_x levels in combination with the non-linear response in O₃ production to decreasing NO_x emissions under the VOC-sensitive MMA airshed (Sierra et al., 2013; Menchaca-Torre et al., 2015).

The O_x long-term trends during 1993–2014 within the MMA were consistent with those for O₃ at all sites. Decreases in NO_x and O₃ observed between 1994 and 1996 were the response to the economic crisis during the same period in Mexico, when the GDP decreased by 5.9 %, providing additional evidence of the dominant role of industries within the MMA. Consistent with economic indicators, annual averaged petrol sales in the Nuevo León State in 1995 decreased by 2.4 % in relation to 1994, but increased linearly from 1996 to 2008 at an approximate rate of 98 800 m³ petrol yr⁻¹ ($r = 0.90$) (Fig. S11) (SENER, 2015). As for petrol sales, registered vehicles in Nuevo León show significant variations between 1993 and 1996 but have increased linearly since 1997 at a rate of around 100 000 vehicles yr⁻¹ ($r = 0.99$). This confirms that despite the annual growth in the vehicular fleet, the fitting of three-way catalyst technology and the reformulation of petrol introduced in 1997 have controlled on-road primary emissions (ProAire-MCMA, 2001). The decreases in NO_x observed at OBI and at all sites during the occurrence of W-SW-NW air masses reflect that if applied, stricter emissions controls such as those for on-road sources can lead to a significant abatement in primary emissions. It is clear that the industrial sources within the MMA must be subject to similar emissions control measures as those implemented within the MCMA for effectively reducing the O₃ levels.

4.5 The opposite O₃ trends in Mexican urban areas

The comparison of O₃ and O_x trends in MMA, GMA, and MCMA reveals different emissions trends at each of the cities studied. The trends in O₃ reported in this study for the MCMA agree with the reduction of 20 ppb O₃ during 1991–2011 for the MCMA (Jaimes et al., 2012), and with the reduction of 8 ppb O₃ during 2000–2011 for the MMA (Benítez-García et al., 2014). In the GMA, the no-trend status in O₃ determined here is in contrast with the increase of 12 ppb O₃ during 2000–2011 (Benítez-García et al., 2014), which is due to the different periods assessed in both studies. Decreases in O₃ in urban US areas arise from effective control of O₃ precursor emissions (Strode et al., 2015), which has occurred at the MCMA.

Figure 10 shows that NO_x decreased significantly within the MCMA (1.57 % yr⁻¹) and the GMA (1.83 % yr⁻¹) during 1993–2014 and 1996–2014, respectively, but increased within the MMA (1.83 % yr⁻¹) during 1993–2014. Such NO_x trends are within the range of the trends in the NO₂ column density reported by Duncan et al. (2016) in Table S9, which reveals an increase of 0.78 ± 1.12 % yr⁻¹ for the MMA, but decreases of 1.82 ± 0.84 % yr⁻¹ for the GMA

and of 0.10 ± 1.67 % yr⁻¹ for the MCMA, all during 2005–2014. To date, long-term trends in VOCs have only been reported in the MCMA, with an average decrease of ca. 2.4 ppb yr⁻¹ since 2002, mostly in propane, ethanol, and acetone (Garzón et al., 2016), while there are no studies of long-term trends in VOCs within the MMA and the GMA.

It has been shown that O₃ and O_x decreases within the MCMA have been driven by reductions in NO_x and VOC emissions and that the implemented strategies described in Sect. 4.1 have proved to be effective in controlling primary emissions (ProAire-MCMA, 2011; Jaimes-Palomera et al., 2016). By contrast, growing industrial emissions within the MMA must be subject to stringent controls to abate O₃ levels. In the GMA, where the industrial activity is lower than in the MCMA and MMA (Kanda et al., 2016), the policies introduced on a national scale for controlling on-road source emissions have resulted in the decrease in NO_x emissions and in the stabilisation of O₃ levels. The results presented here demonstrate the merits of the assessment and analysis of long-term O₃ levels, which can be used by environmental authorities to revise and to redesign programs and policies to improve air quality. Continuing with ground-based O₃ and NO_x monitoring is strongly recommended to better understand the response of changes in primary emissions to further changes in local and regional O₃ levels. Monitoring of VOCs in the GMA and MMA is also recommended since the VOC emissions data reported in the NAEI possess significant uncertainties. Finally, in accordance with the results presented here, we recommend preferentially reducing VOC emissions, which may limit O₃ production in response to a decrease in the VOC/NO_x ratio. However, simultaneously reducing NO_x will have added health benefits of less NO₂.

5 Conclusions

Diurnal and annual cycles and long-term trends in O₃ and O_x within the MMA are interpreted as a response to changes in NO_x and VOCs emissions, photochemistry, and meteorology. Continuous high-frequency and high-precision O₃ and NO_x data recorded during 1993–2014 at five sites within the MMA and at 29 sites within the MCMA and during 1996–2014 at 10 sites within the GMA were used to calculate long-term trends. Within the MMA, the greatest mixing ratios in O₃ were recorded during E and SE winds, at sites downwind of significant precursor emissions from industrial sources. By contrast, the lowest O₃ mixing ratios were recorded at SNN, and for all sites were observed for the W and SW sectors, where air masses travel from central Mexico over 100–300 km of semi-arid and sparsely populated area. Maximum daily 1 h values of O₃ and O_x increased significantly at GPE, SNN, and SNB, owing to increasing emissions of precursors, while at OBI increasing O₃ and decreasing O_x trends arise from the non-linear response to decreasing NO_x emissions from on-road sources.

Annual cycles in O₃ at all sites peak in spring and trough in winter, with a downward spike during summer caused by high winds that disperse O₃ and increase the boundary layer height. Decreases in O₃ precursor emissions during the economic crisis experienced in Mexico between 1994 and 1996 caused significant declining trends in O₃ annual variations from 1993 to 1997 or 1998, depending on the site, followed by significant increases derived from the recovery of the economy. The dominant role of industrial sources in O₃ precursor levels within the MMA was evident at the industrial site SNN during the 1994–1996 economic crisis.

In all metropolitan areas studied, O₃ and O_x levels showed no significant differences between weekdays and the weekend, although an earlier occurrence of the O₃ peak in the GMA was detected, ascribed to a larger VOC/NO_x emissions ratio. The lack of the weekend effect was attributed to weekday O₃ production being limited by VOCs, whereas increases in the VOC/NO_x ratio on weekends in response to reduced emissions from mobile sources resulted in similar O₃ mixing ratios to those during weekdays. Larger AV_d's during weekdays and on weekends were seen in MCMA compared to GMA and MMA, which was related to the relative emissions of the O₃ precursors.

Significant seasonal trends in O₃ and O_x during spring were observed at all sites, apart from STA, whereas industrial sites exhibited significant increases for O_x in all seasons. The largest increases in O₃ and O_x were observed during the occurrence of E-NE-SE air masses. The only significant decrease in O_x at STA was related to the NW wind occurrence during winter. NO_x mixing ratios increased significantly at all sites, except at OBI, due to the dominant role of industrial sources in NO_x levels. The overall significant increasing trend of 0.22 ppb O₃ yr⁻¹ within the MMA contrasts with a significant decreasing trend of 1.15 ppb O₃ yr⁻¹ within the MCMA during 1993–2014, whereas a non-significant trend is evident within the GMA during 1996–2014. At the MCMA and GMA, the overall O_x trends reflect the trends in O₃ precursors. According to the long-term trends in O₃ for the MMA, the number of exceedances of the air quality standards will very likely increase as a result of increasing precursor emissions. The moderate mitigation of O₃ levels within the MCMA, derived from measures implemented to control emissions from on-road, industrial, and area sources, emphasises the need for more stringent control of emissions mostly from industrial sources within the MMA in order to improve air quality. Finally, comparison between emissions inventory estimates of NO_x and VOCs with ground-based measurements indicate that significant reductions in uncertainties are required to better inform air quality policies.

Data availability. The data sets of air pollutants and meteorological parameters used in the present study have been provided in the Supplement.

The Supplement related to this article is available online at <https://doi.org/10.5194/acp-17-9163-2017-supplement>.

Competing interests. The authors declare that they have no conflict of interest.

Acknowledgements. This research was supported by Tecnológico de Monterrey through the Research Group for Energy and Climate Change (grants 0824A0104 and 002EICIR01). Grateful acknowledgements are made to the Secretariat for Sustainable Development of the Nuevo León State, the Secretariat for the Environment of Mexico City, and the Secretariat for the Environment and Territorial Development of the Jalisco State for the public domain records. We gratefully thank the NOAA Air Resources Laboratory (ARL) for access to the HYSPLIT model and READY website (<http://www.ready.noaa.gov>), and we thank Dr. Sigfrido Iglesias for providing the imputed O₃ and NO_x data for the MMA time series. We are also grateful to Professor Paul Monks and Professor Richard Derwent for encouraging comments on an earlier version of the paper.

Edited by: Sally E. Pusede

Reviewed by: two anonymous referees

References

- Akimoto, H., Mori, Y., Sasaki, K., Nakanishi, H., Ohizumi, T., and Itano, Y.: Analysis of monitoring data of ground-level ozone in Japan for long-term trend during 1990–2010: Causes of temporal and spatial variation, *Atmos. Environ.*, 102, 302–310, <https://doi.org/10.1016/j.atmosenv.2014.12.001>, 2015.
- Arriaga-Colina, J. L., West, J. J., Sosa, G., Escalona, S. S., Ordunez, R. M., and Cervantes, A. D. M.: Measurements of VOCs in Mexico City (1992–2001) and evaluation of VOCs and CO in the emissions inventory, *Atmos. Environ.*, 38, 2523–2533, <https://doi.org/10.1016/j.atmosenv.2004.01.033>, 2004.
- Atkinson, R.: Atmospheric chemistry of VOCs and NO_x, *Atmos. Environ.*, 34, 2063–2101, [https://doi.org/10.1016/S1352-2310\(99\)00460-4](https://doi.org/10.1016/S1352-2310(99)00460-4), 2000.
- Benítez-García, S. E., Kanda, I., Wakamatsu, S., Okazaki, Y., and Kawano, M.: Analysis of criteria air pollutant trends in three Mexican metropolitan areas, *Atmosphere*, 5, 806–829, <https://doi.org/10.3390/atmos5040806>, 2014.
- Boersma, K. F., Jacob, D. J., Bucsela, E. J., Perring, A. E., Dirksen, R., van der A, R. J., Yantosca, R. M., Park, R. J., Wenig, M. O., Bertram, T. H., and Cohen, R. C.: Validation of OMI tropospheric NO₂ observations during INTEX-B and application to constrain NO_x emissions over the eastern United States and Mexico, *Atmos. Environ.*, 42, 4480–4497, <https://doi.org/10.1016/j.atmosenv.2008.02.004>, 2008.
- Butler, T. M., Stock, Z. S., Russo, M. R., Denier Van Der Gon, H. A. C., and Lawrence, M. G.: Megacity ozone air quality under four alternative future scenarios, *Atmos. Chem. Phys.*, 12, 4413–4428, <https://doi.org/10.5194/acp-12-4413-2012>, 2012.

- Camalier, L., Cox, W., and Dolwick, P.: The effects of meteorology on ozone in urban areas and their use in assessing ozone trends, *Atmos. Environ.*, 41, 7127–7137, <https://doi.org/10.1016/j.atmosenv.2007.04.061>, 2007.
- Carrillo-Torres, E. R., Hernández-Paniagua, I. Y., and Mendoza, A.: Use of combined observational-and model-derived photochemical indicators to assess the O₃-NO_x-VOC system sensitivity in urban areas, *Atmosphere*, 8, 22, <https://doi.org/10.3390/atmos8020022>, 2017.
- Carslaw, D. C.: The openair manual – open-source tools for analysing air pollution data, Manual for version 1.1-4, King's College London, London, 2015.
- Carslaw, D. C. and Ropkins, K.: openair – an R package for air quality data analysis, *Environ. Modell. Softw.*, 27–28, 52–61, <https://doi.org/10.1016/j.envsoft.2011.09.008>, 2012.
- Castellanos, P. and Boersma, K. F.: Reductions in nitrogen oxides over Europe driven by environmental policy and economic recession, *Sci. Rep.*, 2, 265, <https://doi.org/10.1038/srep00265>, 2012.
- Clapp, L. J. and Jenkin, M. E.: Analysis of the relationship between ambient levels of O₃, NO₂ and NO as a function of NO_x in the UK, *Atmos. Environ.*, 35, 6391–6405, [https://doi.org/10.1016/S1352-2310\(01\)00378-8](https://doi.org/10.1016/S1352-2310(01)00378-8), 2001.
- Cleveland, R. B., Cleveland, W. S., McRae, J., and Terpenning, I.: STL: A seasonal-trend decomposition procedure based on Loess, *J. Off. Stat.*, 6, 3–33, 1990.
- Dentener, F., Stevenson, D., Cofala, J., Mechler, R., Amann, M., Bergamaschi, P., Raes, F., and Derwent, R.: The impact of air pollutant and methane emission controls on tropospheric ozone and radiative forcing: CTM calculations for the period 1990–2030, *Atmos. Chem. Phys.*, 5, 1731–1755, <https://doi.org/10.5194/acp-5-1731-2005>, 2005.
- Duncan, B. N., Lamsal, L. N., Thompson, A. M., Yoshida, Y., Lu, Z., Streets, D. G., Hurwitz, M. M., and Pickering, K. E.: A space-based, high-resolution view of notable changes in urban NO_x pollution around the world (2005–2014), *J. Geophys. Res.*, 121, 976–996, <https://doi.org/10.1002/2015JD024121>, 2016.
- Durbin, J. and Koopman, S. J.: *Time Series Analysis by State Space Methods*, 2nd Edn., Oxford University Press, Oxford UK, 2012.
- EPA (Environmental Protection Agency US): *Compilation of Air Pollution Emission Factors (AP-42)*, Volume I: Stationary Point and Area Sources, available at: <https://www.epa.gov/air-emissions-factors-and-quantification/ap-42-compilation-air-emission-factors> (last access: 14 January 2017), 1995.
- EPA (Environmental Protection Agency US): *User's Guide to MOBILE6.1 and MOBILE6.2: Mobile Source Emission Factor Model*, available at: <https://www3.epa.gov/otaq/models/mobile6/420r03010.pdf> (last access: 16 January 2017), 2003.
- EPA (Environmental Protection Agency US): *Air quality trends*, available at: <https://www.epa.gov/air-trends> (last access: 15 January 2017), 2009.
- Garzón, J. P., Huertas, J. I., Magaña, M., Huertas, M. E., Cárdenas, B., Watanabe, T., Maeda, T., Wakamatsu, S., and Blanco, S.: Volatile organic compounds in the atmosphere of Mexico City, *Atmos. Environ.*, 119, 415–429, <https://doi.org/10.1016/j.atmosenv.2015.08.014>, 2015.
- Guicherit, R. and Roemer, M.: Tropospheric ozone trends, *Chemosphere*, 2, 167–183, [https://doi.org/10.1016/S1465-9972\(00\)00008-8](https://doi.org/10.1016/S1465-9972(00)00008-8), 2000.
- Hernández-Paniagua, I. Y., Lowry, D., Clemitshaw, K. C., Fisher, R. E., France, J. L., Lanoisellé, M., Ramonet, M., and Nisbet, E. G.: Diurnal, seasonal, and annual trends in atmospheric CO₂ at southwest London during 2000–2012: Wind sector analysis and comparison with Mace Head, Ireland, *Atmos. Environ.*, 105, 138–147, <https://doi.org/10.1016/j.atmosenv.2015.01.02>, 2015.
- INE (Instituto Nacional de Ecología): *Cuarto almanaque de datos y tendencias de la calidad del aire en 20 ciudades Mexicanas 2000–2009*, INE-SEMARNAT, México, D. F., 405 pp., 2011.
- INEGI (National Institute of Statistics and Geography): *XIII Censo General de Población y Vivienda 2010*, México, available at: <http://www.censo2010.org.mx/> (last access: 22 May 2016), 2010.
- INEGI (National Institute of Statistics and Geography): *México en Cifras*, México, available at: <http://www3.inegi.org.mx/sistemas/mexicocifras/default.aspxfie=19> (last access: 22 May 2016), 2015.
- INEGI (National Institute of Statistics and Geography): *Producto Interno Bruto (GDP)–Trimestral 2016*, available at: <http://www.inegi.org.mx/est/contenidos/proyectos/cn/pibt/> (last access: 11 January 2017), 2016.
- IPCC: *Climate Change 2013: The Physical Science Basis. Contribution of Working Group I to the Fifth Assessment Report of the Intergovernmental Panel on Climate Change*, 2013, edited by: Stocker, T. F., Qin, D., Plattner, G.-K., Tignor, M., Allen, S. K., Boschung, J., Nauels, A., Xia, Y., Bex, V., and Midgley, P. M., Cambridge University Press, Cambridge, UK and New York, NY, USA, 1535 pp., 2013.
- Jaimes, P. M., Bravo, A. H., Sosa, E. R., Cureño, G. I., Retama, H. A., Granados, G. G., and Becerra, A. E.: Surface ozone concentration trends in Mexico City Metropolitan Area, in: *Proceedings of the Air and Waste Management Association's Annual Conference and Exhibition AWMA*, San Antonio, Texas, 19–22 June 2012, 3, 2273–2284, 2012.
- Jaimes-Palomera, M., Retama, A., Elias-Castro, G., Neria-Hernández, A., Rivera-Hernández, O., and Velasco, E.: Non-methane hydrocarbons in the atmosphere of Mexico City: Results of the 2012 ozone-season campaign, *Atmos. Environ.*, 132, 258–275, <https://doi.org/10.1016/j.atmosenv.2016.02.047>, 2016.
- Jenkin, M. E. and Clemitshaw, K. C.: Ozone and other secondary photochemical pollutants: chemical processes governing their formation in the planetary boundary layer, *Atmos. Environ.*, 34, 2499–2527, [https://doi.org/10.1016/S1352-2310\(99\)00478-1](https://doi.org/10.1016/S1352-2310(99)00478-1), 2000.
- Kanda, I., Basaldud, R., Magaña, M., Retama, A., Kubo, R., and Wakamatsu, S.: Comparison of ozone production regimes between two Mexican cities: Guadalajara and Mexico City, *Atmosphere-Basel*, 7, 91, <https://doi.org/10.3390/atmos7070091>, 2016.
- Lee, Y. C., Shindell, D. T., Faluvegi, G., Wenig, M., Lam, Y. F., Ning, Z., Hao, S., and Lai, C. S.: Increase of ozone concentrations, its temperature sensitivity and the precursor factor in South China, *Tellus B*, 6, 23455, <https://doi.org/10.3402/tellusb.v66.23455>, 2014.
- Lefohn, A. S., Shadwick, D., and Oltmans, S. J.: Characterizing changes in surface ozone levels in metropolitan and rural areas in the United States for 1980–2008 and 1994–2008, *Atmos. Environ.*, 44, 5199–5210, <https://doi.org/10.1016/j.atmosenv.2010.08.049>, 2010.

- Lei, W., de Foy, B., Zavala, M., Volkamer, R., and Molina, L. T.: Characterizing ozone production in the Mexico City Metropolitan Area: a case study using a chemical transport model, *Atmos. Chem. Phys.*, 7, 1347–1366, <https://doi.org/10.5194/acp-7-1347-2007>, 2007.
- Lelieveld, J., Evans, J. S., Fnais, M., Giannadaki, D., and Pozzer, A.: The contribution of outdoor air pollution sources to premature mortality on a global scale, *Nature Lett.*, 525, 367–371, <https://doi.org/10.1038/nature15371>, 2015.
- Menchaca-Torre, H. L., Mercado-Hernández, R., and Mendoza-Domínguez, A.: Diurnal and seasonal variation of volatile organic compounds in the atmosphere of Monterrey, Mexico, *Atmos. Pollut. Res.*, 6, 1073–1081, <https://doi.org/10.1016/j.apr.2015.06.004>, 2015.
- Molina, M. J. and Molina, L. T.: Megacities and atmospheric pollution, *J. Air Waste Manage.*, 54, 644–680, <https://doi.org/10.1080/10473289.2004.10470936>, 2004.
- Monks, P. S.: A review of the observations and origins of the spring ozone maximum, *Atmos. Environ.*, 34, 3545–3561, [https://doi.org/10.1016/S1352-2310\(00\)00129-1](https://doi.org/10.1016/S1352-2310(00)00129-1), 2000.
- Monks, P. S., Archibald, A. T., Colette, A., Cooper, O., Coyle, M., Derwent, R., Fowler, D., Granier, C., Law, K. S., Mills, G. E., Stevenson, D. S., Tarasova, O., Thouret, V., von Schneidemesser, E., Sommariva, R., Wild, O., and Williams, M. L.: Tropospheric ozone and its precursors from the urban to the global scale from air quality to short-lived climate forcer, *Atmos. Chem. Phys.*, 15, 8889–8973, <https://doi.org/10.5194/acp-15-8889-2015>, 2015.
- Parrish, D. D., Millet, D. B., and Goldstein, A. H.: Increasing ozone in marine boundary layer inflow at the west coasts of North America and Europe, *Atmos. Chem. Phys.*, 9, 1303–1323, <https://doi.org/10.5194/acp-9-1303-2009>, 2009.
- Parrish, D. D., Singh, H. B., Molina, L., and Madronich, S.: Air quality progress in North American megacities: A review, *Atmos. Environ.*, 45, 7015–7025, <https://doi.org/10.1016/j.atmosenv.2011.09.039>, 2011.
- PICCA (Programa integral contra la contaminación atmosférica de la zona metropolitana de la Ciudad de México), Mexico City Local Government, available at: http://centro.paot.org.mx/documentos/varioprog_prog_inte_atmosferica.pdf (last access: 28 April 2017), 1990.
- ProAire-MCMA (Programa para Mejorar la Calidad del Aire de la Zona Metropolitana del Valle de México 2002–2010), Mexico City Local Government-State of Mexico Government, available at: http://www.gob.mx/cms/uploads/attachment/file/69312/11_ProAire_ZMVM_2002-2010.pdf (last access: 28 April 2017), 2001.
- ProAire-MMA (Programa de Gestión para Mejorar la Calidad del Aire del Área Metropolitana de Monterrey 2008–2012), SEMARNAT, Gobierno del estado de Nuevo León, available at: http://www.semarnat.gob.mx/archivosanteriores/temas/gestionambiental/calidaddelaire/Documents/Calidad%20del%20aire/Proaires/Proaires_Vigentes/6_ProAire%20AMM%202008-2012.pdf (last access: 22 May 2017), 2008.
- ProAire-MCMA (Programa para Mejorar la Calidad del Aire de la Zona Metropolitana del Valle de México 2002–2010), Mexico City Local Government-State of Mexico Government, available at: <http://www.aire.cdmx.gob.mx/descargas/publicaciones/flippingbook/proaire2011-2020/#p=1> (last access: 28 April 2017), 2011.
- Pugliese, S. C., Murphy, J. G., Geddes, J. A., and Wang, J. M.: The impacts of precursor reduction and meteorology on ground-level ozone in the Greater Toronto Area, *Atmos. Chem. Phys.*, 14, 8197–8207, <https://doi.org/10.5194/acp-14-8197-2014>, 2014.
- Pusede, S. E. and Cohen, R. C.: On the observed response of ozone to NO_x and VOC reactivity reductions in San Joaquin Valley California 1995–present, *Atmos. Chem. Phys.*, 12, 8323–8339, <https://doi.org/10.5194/acp-12-8323-2012>, 2012.
- Pusede, S. E., Steiner, A. L., and Cohen, R. C.: Temperature and recent trends in the chemistry of continental surface ozone, *Chem. Rev.*, 115, 3898–3918, <https://doi.org/10.1021/cr5006815>, 2015.
- R Core Team: R: a Language and Environment for Statistical Computing, R Foundation for Statistical Computing, Vienna, Austria, ISBN 3-900051-07-0, 2013, available at: www.R-project.org (last access: 23 May 2016), 2013.
- Radian (International): Mexico Emissions Inventory Program Manuals (Vol. II-VI), available at: https://www3.epa.gov/ttnatc1/cica/other3_s.html (last access: 15 January 2017), 2000.
- Reinsel, G. C.: Elements of Multivariate Time Series Analysis, 2nd Edn., Springer-Verlag, New York, USA, 1997.
- Revell, L. E., Tummon, F., Stenke, A., Sukhodolov, T., Coulon, A., Rozanov, E., Garny, H., Grewe, V., and Peter, T.: Drivers of the tropospheric ozone budget throughout the 21st century under the medium-high climate scenario RCP 6.0, *Atmos. Chem. Phys.*, 15, 5887–5902, <https://doi.org/10.5194/acp-15-5887-2015>, 2015.
- Rodríguez, S., Huerta, G., and Reyes, H.: A study of trends for Mexico City ozone extremes: 2001–2014, *Atmosfera*, 29, 107–120, <https://doi.org/10.20937/ATM.2016.29.02.01>, 2016.
- Russell, A. R., Valin, L. C., and Cohen, R. C.: Trends in OMI NO₂ observations over the United States: effects of emission control technology and the economic recession, *Atmos. Chem. Phys.*, 12, 12197–12209, <https://doi.org/10.5194/acp-12-12197-2012>, 2012.
- Salmi, T., Määttä, A., Anttila, P., Ruoho-Airola, T., and Amnell, T.: Detecting trends of annual values of atmospheric pollutants by the Mann–Kendall test and Sen’s slope estimates – the Excel template application MAKESENS, Publications on Air Quality Report code FMI-AQ-31, Helsinki, Finland, 31, 1–35, 2002.
- Schultz, M. and Rast, S.: REanalysis of the TROospheric chemical composition over the past 40 years, Emission Data Sets and Methodologies for Estimating Emissions, Work Package 1, Deliverable D1-6, available at: http://retro-archive.iek.fz-juelich.de/data/documents/reports/D1-6_final.pdf (last access: 14 July 2016), 2007.
- SDS (Secretaría de Desarrollo Sustentable): Inventario de emisiones del Área Metropolitana de Monterrey 2013, Monterrey, N. L. México, 4 September 2015.
- SDS (Secretaría de Desarrollo Sustentable): Sistema Integral de Monitoreo Ambiental, available at: <http://aire.nl.gob.mx/>, last access: 21 May 2017.
- SEDEMA (Secretaría del Medio Ambiente): Inventario de Emisiones a la Atmosfera en la ZMVM 1996, available at: <http://www.aire.cdmx.gob.mx/descargas/publicaciones/flippingbook/inventario-emisiones-1996/inventario-de-emisiones-1996.pdf> (last access: 20 May 2017), 1999.

- SEDEMA (Secretaría del Medio Ambiente): Inventario de Emisiones Zona Metropolitana del Valle de México 1998, available at: <http://www.aire.cdmx.gob.mx/descargas/publicaciones/flippingbook/inventario-emisiones-zmvm1998/inventario-emisiones-zmvm1998.pdf> (last access: 20 May 2017), 2001.
- SEDEMA (Secretaría del Medio Ambiente): Inventario de emisiones a la Atmósfera Zona Metropolitana del Valle de México 2000, available at: <http://www.aire.cdmx.gob.mx/descargas/publicaciones/flippingbook/inventario-emisiones-zmvm2000/inventario-emisiones-zmvm2000.pdf> (last access: 20 May 2017), 2003.
- SEDEMA (Secretaría del Medio Ambiente): Inventario de emisiones de la Zona Metropolitana del Valle de México 2002, available at: <http://www.aire.cdmx.gob.mx/descargas/publicaciones/flippingbook/inventario-emisiones-zmvm2002/inventario-emisiones-zmvm2002.pdf> (last access: 20 May 2017), 2004.
- SEDEMA (Secretaría del Medio Ambiente): Inventario de Emisiones Zona Metropolitana del Valle de México 2004, available at: <http://www.aire.cdmx.gob.mx/descargas/publicaciones/flippingbook/inventario-emisiones-zmvm-criterio2004/inventario-emisiones-zmvm-criterio2004.pdf> (last access: 20 May 2017), 2006.
- SEDEMA (Secretaría del Medio Ambiente): Inventario de Emisiones de Contaminantes Criterio 2006, available at: <http://www.aire.cdmx.gob.mx/descargas/publicaciones/flippingbook/inventario-emisiones-zmvm-criterio2006/inventario-emisiones-zmvm-criterio2006.pdf> (last access: 20 May 2017), 2008.
- SEDEMA (Secretaría del Medio Ambiente): Inventario de emisiones de contaminantes criterio de la ZMVM 2008, available at: <http://www.aire.cdmx.gob.mx/descargas/publicaciones/flippingbook/inventario-emisiones-zmvm-criterio-2010/inventario-emisiones-zmvm-criterio2010.pdf> (last access: 20 May 2017), 2010.
- SEDEMA (Secretaría del Medio Ambiente): Inventario de emisiones de la Zona Metropolitana del Valle de México contaminantes criterio 2010, available at: <http://www.aire.cdmx.gob.mx/descargas/publicaciones/flippingbook/inventario-emisioneszmvm2012/inventario-emisioneszmvm2012.pdf> (last access: 20 May 2017), 2012.
- SEDEMA (Secretaría del Medio Ambiente): Inventario de Emisiones Contaminantes y de efecto invernadero, available at: <http://www.aire.cdmx.gob.mx/descargas/publicaciones/flippingbook/inventario-emisiones-cdmx2014-2/IE-CDMX-2014.pdf> (last access: 20 May 2017), 2014.
- SEDEMA (Secretaría del Medio Ambiente de la Ciudad de México): Sistema de Monitoreo Atmosférico, available at: <http://www.aire.df.gob.mx/default.php> (last access: 21 May 2016), 2016a.
- SEDEMA (Secretaría del Medio Ambiente de la Ciudad de México): Inventario de Emisiones de la CDMX 2014 Contaminantes Criterio Tóxicos y de Efecto Invernadero, available at: <http://www.aire.cdmx.gob.mx/descargas/publicaciones/flippingbook/inventario-emisiones-cdmx2014-2/> (last access: 10 January 2017), 2016b.
- SEMARNAT (Secretaría del Medio Ambiente y Recursos Naturales): NOM-041 (Norma Oficial Mexicana, que establece los límites máximos permisibles de emisión de gases contaminantes provenientes del escape de los vehículos automotores en circulación que usan gasolina como combustible), Diario Oficial de la Federación, 1993a.
- SEMARNAT (Secretaría del Medio Ambiente y Recursos Naturales): NOM-042 (Norma Oficial Mexicana que establece los límites máximos permisibles de emisión de hidrocarburos totales o no metano, monóxido de carbono, óxidos de nitrógeno y partículas provenientes del escape de los vehículos automotores nuevos cuyo peso bruto vehicular no exceda los 3,857 kilogramos, que usan gasolina, gas licuado de petróleo, gas natural y diesel, así como de las emisiones de hidrocarburos evaporativos provenientes del sistema de combustible de dichos vehículos), Diario Oficial de la Federación, 1993b.
- SEMARNAT (Secretaría del Medio Ambiente y Recursos Naturales): Inventario Nacional de Emisiones 1999, México, D. F., available at: <http://www.inecc.gob.mx/dica/548-calaire-inem-1999> (last access: 20 May 2017), 2006.
- SEMARNAT (Secretaría del Medio Ambiente y Recursos Naturales): Inventario Nacional de Emisiones 2005, México, D. F., available at: <http://sinae.semarnat.gob.mx/sinae.php?steprep=5&process=UkVQT1JURUFET1I=&r=NC4gRnV1bnRlIHkgRW50aWRhZGVzIEZlZGVyYXRpd mFz> (last access: 22 May 2017), 2011.
- SEMARNAT (Secretaría del Medio Ambiente y Recursos Naturales): Inventario Nacional de Emisiones 2008, México, D. F., available at: <http://sinae.semarnat.gob.mx/sinae.php?steprep=5&process=UkVQT1JURUFET1I=&r=NC4gRnV1bnRlIHkgRW50aWRhZGVzIEZlZGVyYXRpd mFzIDlwMDgu> (last access: 22 May 2017), 2014.
- SEMARNAT (Secretaría del Medio Ambiente y Recursos Naturales): Informe Nacional de calidad del aire 2014, México, D. F., available at: <http://sinaica.inecc.gob.mx/archivo/informes/Informe2014.pdf> (last access: 15 December 2017), 2015.
- SENER (Secretaría de Energía): Estadísticas Energéticas Nacionales, México, available at: <http://sie.energia.gob.mx/> (last access: 12 July 2017), 2016.
- Sicard, P., Serra, R., and Rossello, P.: Spatiotemporal trends in ground-level ozone concentrations and metrics in France over the time period 1999–2012, *Environ. Res.*, 149, 122–144, <https://doi.org/10.1016/j.envres.2016.05.014>, 2016.
- Sierra, A., Vanoye, A. Y., and Mendoza, A.: Ozone sensitivity to its precursor emissions in northeastern Mexico for a summer air pollution episode, *J. Air Waste Manage.*, 63, 1221–1233, <https://doi.org/10.1080/10962247.2013.813875>, 2013.
- Simon, H., Reff, A., Wells, B., Xing, J., and Frank, N.: Ozone trends across the United States over a period of decreasing NO_x and VOC emissions, *Environ. Sci. Technol.*, 49, 186–195, <https://doi.org/10.1021/es504514z>, 2015.
- SMN (Servicio Meteorológico Nacional), available at: <http://smn.cna.gob.mx/es/>, last access: 21 May 2016.
- Stahelin, J. and Schmid, W.: Trend analysis of tropospheric ozone concentrations utilizing the 20 year data set of ozone balloon soundings over Payerne (Switzerland), *Atmos. Environ.*,

- 25, 1739–1749, [https://doi.org/10.1016/0960-1686\(91\)90258-9](https://doi.org/10.1016/0960-1686(91)90258-9), 1991.
- Stein, A. F., Draxler, R. R., Rolph, G. D., Stunder, B. J. B., Cohen, M. D., and Ngan, F.: NOAA'S HYSPLIT atmospheric transport and dispersion modelling system, *B. Am. Meteorol. Soc.*, 96, 2059–2077, <https://doi.org/10.1175/BAMS-D-14-00110.1>, 2015.
- Stephens, S., Madronich, S., Wu, F., Olson, J. B., Ramos, R., Retama, A., and Muñoz, R.: Weekly patterns of México City's surface concentrations of CO, NO_x, PM₁₀ and O₃ during 1986–2007, *Atmos. Chem. Phys.*, 8, 5313–5325, <https://doi.org/10.5194/acp-8-5313-2008>, 2008.
- Stevenson, D. S., Dentener, F. J., Schultz, M. G., Ellingsen, K., van Noije, T. P. C., Wild, O., Zeng, G., Amann, M., Ahernton, C. S., Bell, N., Bergmann, D. J., Bey, I., Butler, T., Cofala, J., Collins, W. J., Derwent, R. G., Doherty, R. M., Drevet, J., Eskes, H. J., Fiore, A. M., Gauss, M., Hauglustaine, D. A., Horowitz, L. W., Isaksen, I. S. A., Krol, M. C., Lamarque, J.-F., Lawrence, M. G., Montanaro, V., Müller, J.-F., Pitari, G., Prather, M. J., Pyle, J. A., Rast, S., Rodriguez, J. M., Sanderson, M. G., Savage, N. H., Shindell, D. T., Strahan, S. E., Sudo, K., and Szopa, S.: Multimodel ensemble simulations of present-day and near-future tropospheric ozone, *J. Geophys. Res.-Atmos.*, 111, D08301, <https://doi.org/10.1029/2005JD006338>, 2006.
- Strode, S. A., Rodriguez, J. M., Logan, J. A., Cooper, O. R., Witte, J. C., Lamsal, L. N., Damon, M., Van Aartsen, B., Steenrod, S. D., and Strahan, S. E.: Trends and variability in surface ozone over the United States, *J. Geophys. Res.*, 120, 9020–9042, <https://doi.org/10.1002/2014JD022784>, 2015.
- Tiwari, A. K., Suresh, K. G., Arouri, M., and Teulon, F.: Causality between consumer price and producer price: Evidence from Mexico, *Econ. Model.*, 36, 432–440, <https://doi.org/10.1016/j.econmod.2013.09.050>, 2014.
- Torres-Jardon, R., García-Reynoso, J. A., Jazcilevich, A., Ruiz-Suárez, L. G., and Keener, T. C.: Assessment of the ozone-nitrogen oxide-volatile organic compound sensitivity of Mexico City through an indicator-based approach: measurements and numerical simulations comparison, *J. Air Waste Manage.*, 59, 1155–1172, <https://doi.org/10.3155/1047-3289.59.10.1155>, 2009.
- VanCuren, R.: Transport aloft drives peak ozone in the Mojave Desert, *Atmos. Environ.*, 109, 331–341, <https://doi.org/10.1016/j.atmosenv.2014.09.057>, 2015.
- Velasco, E., Lamb, B., Westberg, H., Allwine, E., Sosa, G., Arriaga-Colina, J. L., Jobson, B. T., Alexander, M. L., Prazeller, P., Knighton, W. B., Rogers, T. M., Grutter, M., Herndon, S. C., Kolb, C. E., Zavala, M., de Foy, B., Volkamer, R., Molina, L. T., and Molina, M. J.: Distribution, magnitudes, reactivities, ratios and diurnal patterns of volatile organic compounds in the Valley of Mexico during the MCMA 2002 & 2003 field campaigns, *Atmos. Chem. Phys.*, 7, 329–353, <https://doi.org/10.5194/acp-7-329-2007>, 2007.
- Vingarzan, R.: A review of surface ozone background levels and trends, *Atmos. Environ.*, 38, 3431–3442, <https://doi.org/10.1016/j.atmosenv.2004.03.030>, 2004.
- Wang, Y., Konopka, P., Liu, Y., Chen, H., Müller, R., Plöger, F., Riese, M., Cai, Z., and Lü, D.: Tropospheric ozone trend over Beijing from 2002–2010: Ozone-sonde measurements and modeling analysis, *Atmos. Chem. Phys.*, 12, 8389–8399, <https://doi.org/10.5194/acp-12-8389-2012>, 2012.
- Wilson, R. C., Fleming, Z. L., Monks, P. S., Clain, G., Henne, S., Konovalov, I. B., Szopa, S., and Menut, L.: Have primary emission reduction measures reduced ozone across Europe? An analysis of European rural background ozone trends 1996–2005, *Atmos. Chem. Phys.*, 12, 437–454, <https://doi.org/10.5194/acp-12-437-2012>, 2012.
- Wolff, G. T., Kahlbaum, D. F., and Heuss, J. M.: The vanishing ozone weekday/weekend effect, *J. Air Waste Manage.*, 63, 292–299, <https://doi.org/10.1080/10962247.2012.749312>, 2013.
- World Health Organization: Ambient (outdoor) air quality and health, 2014 update, available at: <http://www.who.int/mediacentre/factsheets/fs313/en/>, last access: 21 May 2016.
- Xing, J., Pleim, J., Mathur, R., Pouliot, G., Hogrefe, C., Gan, C.-M., and Wei, C.: Historical gaseous and primary aerosol emissions in the United States from 1990 to 2010, *Atmos. Chem. Phys.*, 13, 7531–7549, <https://doi.org/10.5194/acp-13-7531-2013>, 2013.
- Xu, X., Lin, W., Wang, T., Yan, P., Tang, J., Meng, Z., and Wang, Y.: Long-term trend of surface ozone at a regional background station in eastern China 1991–2006: Enhanced variability, *Atmos. Chem. Phys.*, 8, 2595–2607, <https://doi.org/10.5194/acp-8-2595-2008>, 2008.
- Zellweger, C., Hüglin, C., Klausen, J., Steinbacher, M., Vollmer, M., and Buchmann, B.: Inter-comparison of four different carbon monoxide measurement techniques and evaluation of the long-term carbon monoxide time series of Jungfraujoch, *Atmos. Chem. Phys.*, 9, 3491–3503, <https://doi.org/10.5194/acp-9-3491-2009>, 2009.
- Zheng, J., Swall, J. L., Cox, W. M., and Davis, J. M.: Interannual variation in meteorologically adjusted ozone levels in the eastern United States: A comparison of two approaches, *Atmos. Environ.*, 41, 705–716, <https://doi.org/10.1016/j.atmosenv.2006.09.010>, 2007.